

Morphological Characterization of Blends of Metal-Sulfonated Poly(styrene) and a Methylated Poly(amide) by Solid State NMR

D. L. VanderHart,[†] Y. Feng,^{†,§} C. C. Han,[†] and R. A. Weiss[‡]

Polymers Division, National Institute of Standards and Technology, Gaithersburg, Maryland 20899, and Polymer Science Program and Department of Chemical Engineering, University of Connecticut, Storrs, Connecticut 06269-3136

Received September 13, 1999; Revised Manuscript Received December 2, 1999

ABSTRACT: Various blends of atactic, low-MW (≈ 4000), metal-sulfonated poly(styrene) (MSPS) and a higher-MW ($\approx 25\,000$) poly(amide) (PA) were studied by solid-state ^{13}C and proton NMR techniques which include multiple-pulse irradiation, cross-polarization, and magic angle spinning. This study is an investigation of the morphology of these MSPS(n)/PA blends ($n = 100 \times \text{mole fraction sulfonate} = 2.3, 7.0, \text{ or } 11.9$) as functions of blend composition and sulfonation level. Unsulfonated PS and PA are incompatible and phase separate. Decoration with sulfonate groups promotes mixing of the blend components owing to strong, polar metal-sulfonate/amide interactions. Metal ions used were divalent Zn (diamagnetic) and Cu (paramagnetic), the latter ions having a significant influence on the protons. The PA, *N,N*-dimethylethylene sebacamide, was *N*-methylated to weaken interactions between PA chains, thereby promoting mixing. Pure PA is semicrystalline, and intimate mixing prevents PA crystallization. ^{13}C CPMAS spectra were used to assay PA crystallinity. The stability of the blend morphology in the presence of water was also studied since water is expected to modify or compete with the polar interactions of the blend. Many of the experiments performed relied, for their interpretation, on the phenomenon of proton spin diffusion. For ZnSPS(11.9)/PA blends, mixing was quite intimate and PA crystallinity was suppressed for PA mass fractions of 0.5 and lower. PA crystallinity first appeared with a PA mass fraction of 0.65; however, this crystallinity was not the result of large-scale phase separation of the PA from the MSPS. Rather, PA crystallinity develops in the mixed MSPS/PA phase in such a way that each PA crystallite is surrounded by a mixed MSPS/PA phase. Larger PA mass fractions gave higher PA crystallinities. When PA crystallinity is present, there is an average periodicity of about 20–25 nm; moreover, the noncrystalline regions surrounding each crystallite have nonuniform composition in the sense that there is a buffer zone adjacent to the PA crystallites which is mainly PA in composition. A few blends involving ZnSPS(7.0) and ZnSPS(2.3) were also studied. Only the 75/25 ZnSPS(7.0)/PA blend seemed well mixed and noncrystalline. Compositional heterogeneities on scales larger than 20 nm were seen in the remaining blends. Certain CuSPS ionomers and blends, analogous to the Zn-containing materials, were studied in an attempt to resolve some ambiguities present in the interpretation of the data taken for the Zn-containing materials. Zn and Cu ions show similar affinities for the amide moieties; hence, the morphology for analogous Zn- and Cu-containing blends is expected to be similar. Mainly proton longitudinal relaxation was measured because it is sensitive to the presence of paramagnetic Cu. Two matters were pursued for the Cu-containing materials: First, the uniformity of Cu distribution was probed in pure CuSPS(11.9). Our T_1^{H} analysis gave a variation by a factor of 1.3 in averaged Cu concentration, where the averaging was done over dimensions of 14 nm. Second, given that the 75/25 CuSPS(2.3)/PA blend exhibits large-scale phase separation, where one phase contains nearly all of the PA plus a small fraction of the SPS, we addressed the question whether the level of decorations for the SPS chains in this mixed phase was significantly above the 2.3% average. Our analysis did not support such a claim within the assumption that the morphologies of the Zn- and Cu-containing blends are the same. Toward an evaluation of paramagnetic Cu ions as aids for the elucidation of morphology in organic systems, several qualitative characteristics of the proton and ^{13}C relaxation are noted for these Cu-containing materials. Also, an estimate of the electron relaxation time, T_1^{e} , in CuSPS(11.9) is given as is the fraction (0.95) of observable protons using multiple-pulse techniques. T_1^{e} is shown to vary strongly with overall Cu concentration in the pure ionomers and with the amount of water absorbed in the pure ionomer. T_1^{e} also changes when Cu is bound to the amide moiety of PA. One cannot simply assume that the average Cu concentration and $(1/T_1^{\text{H}})$ are proportional. A few annealing experiments also indicate that when the mole fraction of Cu is 7.0% or 2.3% in the ionomer, annealing seems to promote more clustering as though the cast films were not at their energy minima with respect to Cu–Cu interactions. Finally, in CuSPS(11.9), spin diffusion results indicate that the position of the SAXS maximum near $q = 2 \text{ nm}^{-1}$ is consistent with the separation between paramagnetic centers, which centers, in turn, are estimated to consist of clusters of about 10 Cu sites. If cluster size diminishes with average Cu concentration, then data indicate that T_1^{e} is a strong function of cluster size.

Introduction

Polyamides (nylons) constitute an important class of thermoplastics noted for their toughness, high modulus,

and high tensile strength.¹ They are used in a wide variety of applications as structural plastics and as reinforcing fibers in high-performance composites. The improvement of various mechanical, rheological, and other properties of these materials, therefore, has been of much academic as well as commercial interest.

Polyamides contain amide groups along the polymer backbone. These groups are responsible for significant

[†] National Institute of Standards and Technology.

[‡] University of Connecticut.

[§] Current address: Corporate Research Division, Goodyear Tire and Rubber Co., 142 Goodyear Blvd., Akron, OH 44305-0001.

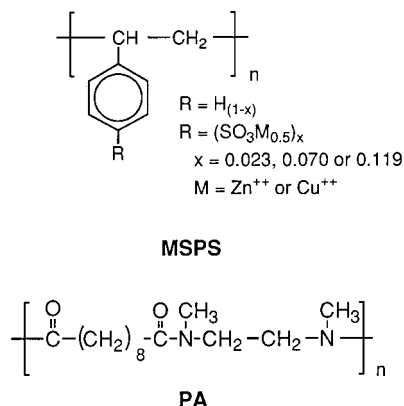


Figure 1. Chemical structures for the blend components.

interchain interactions. At the same time, the amide group is a site amenable to specific interactions with other polymers. Therefore, a general approach for compatibilizing polyamides with other polymers is to introduce functional groups into the second component to promote intermolecular interactions.²⁻⁴ Metal sulfonate groups have often been used for this purpose since they can be incorporated, in controlled amounts,⁵⁻⁷ into a number of polymers; moreover, various metals can be used as the counteragent to form complexes of different strengths.⁸⁻¹¹

For blends of polymers containing metal sulfonate groups with various commercial nylons, such as nylon-6, the amide hydrogen is capable of hydrogen bonding with the carbonyl group as well as with the sulfonate group. These associations between amide groups compete with the metal–amide interactions so that a description of overall intermolecular interactions becomes complex; moreover, miscibility is achieved over only a limited range of blend stoichiometries. To simplify matters, our approach in this study was to remove the potential for hydrogen bonding between polyamide segments by using an *N,N*-methylated polyamide, namely, poly(*N,N*-dimethylethylene sebacamide), which we will simply refer to as “PA”. The corresponding metal-sulfonate polymers we used were polystyrenes having three different levels of sulfonation. Chemical formulas for both the PA and the metal-sulfonated poly(styrene)’s (MSPS) are shown in Figure 1.

The effects of intermolecular interactions in polymer blends with regard to the enhancement of miscibility and final properties have been reported in many studies. Included in these reports are the study of thermal–mechanical properties using DSC or DMTA⁸⁻¹¹ and morphological characterization using SEM.¹² Thermal–mechanical tests probe overall miscibility on a scale larger than 15 nm. In addition, some solid-state NMR studies were carried out.¹²⁻¹⁴ In those NMR studies, proton spin–lattice relaxation times^{13,14} and intermolecular cross-polarization¹⁵ were used. The latter technique offers insights into the mixing of the components of a blend on a distance scale about 0.6 nm; however, selective deuteration of one of the blend components is required.

PA crystallinity is an important part of the characterization of these blends of PA with ZnSPS or with CuSPS. Crystallization of the PA competes with the compatibilizing influence of the methylated-amide/metal-sulfonate interaction. In fact, at ambient temperature, fully crystalline PA, phase separated from the ionomer, probably represents the (unattainable) free energy

minimum. ¹³C NMR utilizing cross-polarization (CP) and magic-angle spinning (MAS) allows one to identify and quantify the level of crystallinity of the PA fraction. One implication of *N*-methylation is that the crystallization rates of the PA used in this study are relatively slow, and T_g is much lower compared to that of the analogous non-methylated nylon. Intuitively, one expects that for a given blend stoichiometry there should be a threshold number of methylated-amide/metal-sulfonate interactions above which PA crystallization would be completely inhibited. It is also intuitive that the stability of the bonds formed between the methylated amide and the metal sulfonate also plays an important role in the development of PA crystallinity and the stability of the blend morphology. Given the excess number of amide versus metal-sulfonate groups in the blends we examined, if these intermolecular bonds broke up and re-formed at any significant rate, one could imagine that a mechanism for slow PA crystallization could exist. The role of water, as an agent for weakening these bonds, is important in this context. A very limited look at aging is included in this paper.

Solid-state proton NMR, mostly involving multiple-pulse methods,¹⁶⁻¹⁸ forms the basis of most of the experiments reported herein. The chemical-shift-based (CSB) proton spin diffusion methodology¹⁹⁻²² applied to the study of the blends of ZnSPS and PA in this paper offers insights into the distance scale of compositional heterogeneity; at the same time, there is a limited amount of information available about the stoichiometry of the mixed phases. $T_{1\rho}$ -based spin diffusion experiments²³ ($T_{1\rho}$ is a relaxation time²⁴ under MREV-8^{17,18} multiple-pulse irradiation) offer further clarification about morphology when PA crystallinity is present. In addition, qualitative insights into the uniformity of cation distribution in the pure ionomers and into the existence, or nonexistence, of large, pure-PA domains in certain blends is obtained through the use of Cu^{2+} , a paramagnetic cation which influences²⁵ the longitudinal relaxation of the protons in CuSPS and its PA blends.

Experimental Section

Materials. Poly(*N,N*-dimethylethylene sebacamide) (PA) was prepared by a nucleophilic acyl substitution reaction of sebacoyl chloride with *N,N*-dimethylethylenediamine in the presence of tetrachloroethylene and a 50% excess of pyridine.²⁶ The resulting PA was washed first with water and then heptane. The number-average and mass-average molecular masses measured by gel permeation chromatography were 25 and 65 kg/mol, respectively, based on polystyrene standards. PA has a glass transition temperature (T_g) of about 0 °C and a melting point, T_m , of about 75 °C.

Lightly sulfonated polystyrene ionomers (SPS) were prepared by sulfonating a narrow molecular mass distribution polystyrene (Pressure Chemical Co.;²⁷ $M_n = 4000$ g/mol, $M_w/M_n = 1.06$) with acetyl sulfate in 1,2-dichloroethane at 50 °C.²⁸ This particular reaction produces random substitution along the chain primarily at the para position on the phenyl ring. The sulfonation level was determined by titration of the free acid derivative, HSPS, in mixed toluene/methanol solvent of volume ratio 90/10. HSPS samples were made whose sulfonation levels, expressed as mole fractions referenced to the moles of PS repeat units, were 2.3%, 7.0%, and 11.9%. Zinc and copper salts were prepared by neutralizing the HSPS in a toluene/methanol solution with a 20% excess of the metal acetate dissolved in methanol. The ionomer salts were then isolated from solution by steam stripping and filtration, followed by washing several times with deionized water and drying under vacuum. The ionomer nomenclature used in this paper is MSPS(*n*), where M denotes the metal cation and *n* is

the mole percent of PS monomers whose rings are sulfonated, usually at the para position.

Blends of the MSPS ionomers with the PA were prepared by first dissolving the two components in a mixture of methanol and dichloroethane (10/90 in volume ratio), casting a film in a Teflon dish, drying in a vacuum oven overnight at 130 °C, and then transferring into an NMR rotor for solid-state NMR measurements. Compositions of blends are expressed as mass ratios.

Proton NMR measurements were conducted at ambient temperature and 4.7 T (200.05 MHz) on a Bruker CXP200 spectrometer. The MAS proton probe was manufactured by Doty Scientific and features a 5 mm o.d. sapphire rotor. Samples with a maximum height of 2.5 mm were centered in the rotor. Spinning speeds were 2604 ± 10 Hz unless otherwise noted. The rf amplitude corresponded to $1.5 \mu\text{s}$ 90° pulses. The basic multiple-pulse cycle utilized was the MREV-8^{17,18} cycle where the overall cycle time was $38.4 \mu\text{s}$. Specific pulse sequences are discussed in connection with the results.

¹³C NMR spectra were conducted at ambient temperature and 2.35 T (25.19 MHz) on a noncommercial spectrometer utilizing a noncommercial probe whose rotor/stator assembly was manufactured by Doty Scientific. The MAS frequency was 4 kHz; the proton and ¹³C rf levels used in cross-polarization and decoupling corresponded to nutation frequencies of 66 and 70 kHz, respectively. The cross-polarization time was 0.7 ms.

The small-angle X-ray scattering patterns were collected on an apparatus at N.I.S.T. This instrument uses Cu K α radiation and is equipped with a 10 m beam path and a 2-D detector. Cylindrical averaging about the beam direction was employed to generate the 1-D scattering patterns. Samples were in the form of thick films, about 1 mm thick. Corrections were applied to the data based on empty-beam measurements and on measurements of the attenuation factor of the sample of interest.

Results

Two important perspectives should be kept in mind as the results and discussion are presented. First, this study is exploratory and not a systematic study; therefore, certain topics will be addressed in an incomplete manner. Second, the emphasis of this study is the elucidation of morphology. Because the morphology of these materials can become quite complex, especially when PA crystallization also occurs, and because NMR spin diffusion methods are relatively crude probes of morphology, compared with direct imaging techniques, the interpretations of the data will often leave ambiguities. That is the nature of this method applied to a complex system. However, one important strength of the NMR method is that compositional information is available also. When one is trying to characterize phases of mixed composition, the insights that NMR can provide are quite unique compared to other techniques, especially when one considers the small distance scale, 3–4 nm, that NMR spin diffusion techniques are sensitive to.

The ¹³C Spectrum of Crystalline PA. Since one of the important thermodynamic considerations in the ZnSPS/PA blends is the possibility that the PA material crystallizes, we begin by isolating the ¹³C NMR spectrum of the crystalline (CR) and noncrystalline (NC) phases for a sample of pure PA that had been stored at ambient conditions for several months and dried in a vacuum. Figure 2 shows two experimental spectra along with two other spectra representing the CR and NC phases of the PA. The latter spectra are linear combinations of the two experimental spectra, which, in turn, differ only in the time of proton spin locking (1 μs or 5 ms) which occurs prior to cross-polarization. Since the proton relaxation time, $T_{1\rho}^H$, during spin locking is

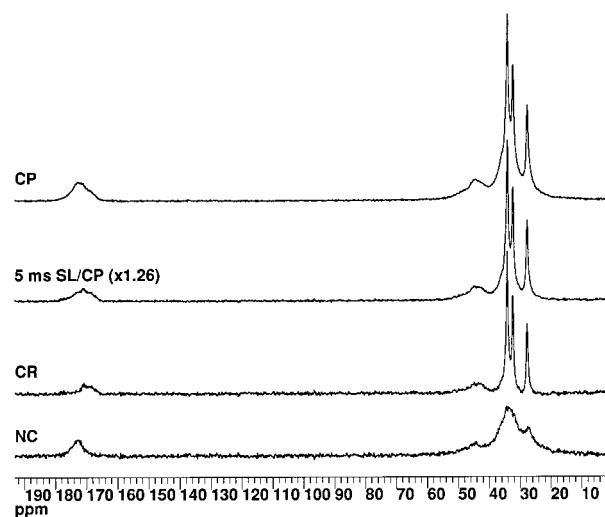


Figure 2. Method for isolating the 25 MHz ¹³C CPMAS spectra of the crystalline (CR) and noncrystalline (NC) regions of pure PA. CP time is 0.7 ms. Upper two spectra are experimental: proton spin-locking times preceding CP are 1 μs and 5 ms; intensity ratios for the CR and NC spectra change with locking time. Spectra designated “CR” and “NC” are the line shapes deduced for the crystalline and the noncrystalline regions using linear combinations of the experimental spectra. Note the sharp spectral signature of the three lines in the 25–36 ppm range in the “CR” spectrum.

different for the CR and NC phases, the relative signal strength arising from these two regions varies in these two spectra. Hence, one can take appropriate linear combinations of these experimental spectra²⁹ in order to isolate the spectra of the CR and NC phases. In this case, as is usual, the resonances of the CR region show superior resolution and a longer $T_{1\rho}^H$; the linear combinations chosen are based on these characteristics. A crude estimate of the $T_{1\rho}^H$'s, based on the attenuation of each signal over 5 ms of spin locking, is 4.4 and 21 ms for the protons in the NC and CR regions, respectively. Note that the spectrum of the CR region, Figure 2c, also has two rather broad resonances: the methylene carbon at about 43 ppm and the carbonyl carbon near 170 ppm. These resonances are not so sharp as the other methylene resonances principally because the former carbons are adjacent to the quadrupolar ¹⁴N nucleus which gives rise to spectral broadening.^{30,31} Note also the downfield shift of the carbonyls in the NC region, relative to carbons in the CR phase. The important deduction of Figure 2 is the identification of the sharp, high-field features with the crystalline phase of the PA. These features will serve as indicators for crystalline PA.

¹³C Spectra of the Blends. Figure 3 shows ¹³C spectra of various vacuum-dried blends after aging for at least a week at ambient temperature following their preparation. One can tell by inspection whether crystalline PA is present. The spectra of the 75/25 ZnSPS-(11.9)/PA, 75/25 ZnSPS(7.0)/PA, and 50/50 ZnSPS(11.9)/PA samples all lack evidence of a PA CR phase. The remainder all show some level of crystallinity, and judging by the integrated intensity ratio of the sharp features to the broader underlying intensity in the PA region between 20 and 38 ppm, one can recognize that the 35/65 ZnSPS(11.9)/PA sample has the lowest crystallinity and the 75/25 ZnSPS(2.3)/PA, 25/75 ZnSPS-(7.0)/PA, and 18/82 ZnSPS(11.9)/PA samples have higher levels of crystallinity. One can use the CR spectrum of Figure 2c to estimate the crystalline fraction, f_c^{PA} , of the

Table 1. Morphological Deductions, Proton Longitudinal Relaxation Times (T_1^H), and Fractions (f_c^{PA}) of the PA Component in the Crystalline State for Various Pure Materials and Zn-Containing Blends

sample stoichiometry ZnSPS/PA (mass %)	SO ₃ decoration (mole fraction of PS, %)	f_c^{PA} ^a	T_1^H ^b (ms)	morphology ^c
100/0	0.0		1530	GL
100/0	2.3		1410	GL
100/0	7.0		671	GL
100/0	11.9		928	GL
75/25	2.3	0.32(3)	1410, 743	PhSep, SC(>200/PSr)
75/25	7.0	<0.02	772	GL, int mix
75/25	11.9	<0.01	815	GL, int mix
58/42	0.0	0.40(3)	1540, 923	phys mix (GL, SC)
50/50	11.9	<0.01	757	GL, int mix
35/65	11.9	0.07(2)	649	PhSep, SC(not det)
25/75	7.0	0.25(3)	812	PhSep, SC(25, >200)
25/75	11.9	0.12(2)	955	PhSep, SC(25)
18/82	11.9	0.19(2)	805	PhSep, SC(25)
18/82 (aged: 14 months)	11.9	0.26(3)	965	PhSep, SC(not det)
18/82 (wet/dried)	11.9	0.42(3)	1070	PhSep, SC(25)
0/100 (initial)		?	584	SC
0/100 (6 days)		?	952	SC
0/100 (2 weeks)		0.39(3)	?	SC

^a f_c^{PA} = fraction of crystallinity, normalized to the total PA present. Numbers in parentheses are estimates of the full range of uncertainty for the last decimal place. ^b Two values for T_1^H indicate that T_1^H nulls associated with both the PS and the PA signals could be detected; the first value is associated with the PS component. An estimate of the expanded uncertainty for these values is $\pm 5\%$ of the given value for single numbers and $\pm 10\%$ for situations where two values are given. ^c Codes for morphology: "GL" = glassy, "SC" = semicrystalline, "phys mix" = physical mixture, "PhSep" = phase separated, numbers in parentheses are characteristic distance scales, in nm, over which chemical heterogeneity is detected, "not det" = not determined, "PSr" means that the least mixed phase is PS-rich.

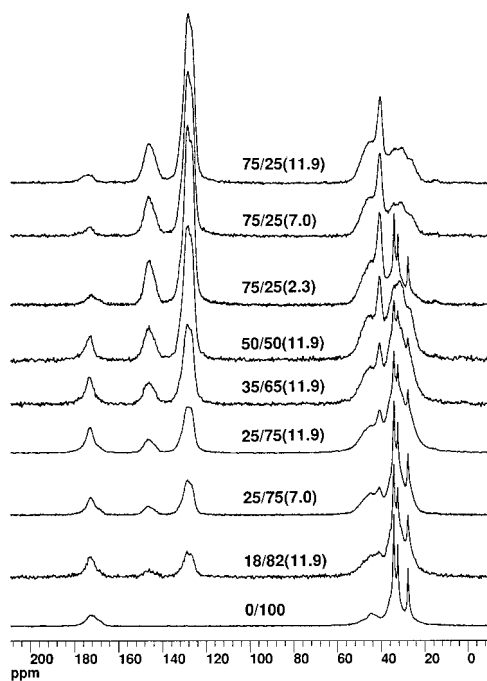


Figure 3. The 25 MHz CPMAS spectra of various blends. Vertical scales are chosen for convenience of display; total integrals vary.

total PA in these spectra. Table 1 summarizes these findings along with other morphological information that is, in part, based on data and discussion to be presented. One general trend is that crystallinity of PA increases as the density of sulfonate groups decreases via either a decrease in the MSPS mass fraction or a decrease in the mole fraction of sulfonate groups in the MSPS.

Figure 4 shows a comparison of PS spectra where we are looking for spectral differences associated with sulfonation versus no sulfonation. Spectra for pure PS and for ZnSPS(11.9) are shown along with the difference spectrum. In the spectrum of the ZnSPS(11.9) two effects appear, both of them rather subtle. First, the

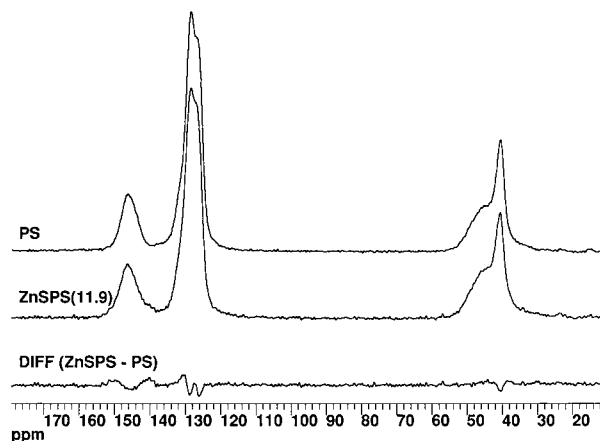


Figure 4. CPMAS spectra of atactic poly(styrene): undecorated (PS) and decorated (ZnSPS(11.9)); the difference spectrum is also shown. Total intensities in the upper two spectra are equal. Sulfonate substitution is a weak spectral perturbation.

spectral resolution seems slightly poorer, and second, a weak shoulder appears at about 140 ppm; the latter shows up also as a small peak in the difference spectrum although it is by no means the only feature. This shoulder has been identified previously³² with the aromatic carbon at the site of sulfonation in these materials. The reason for the slightly degraded resolution is not apparent; it may be associated with a different conformational distribution of the PS backbone as a result of the aggregation of the zinc sulfonate moieties, but this is speculative. Figure 4 also demonstrates that when the mass fraction of sulfonate groups is 12% or less, the ¹³C spectra will not be very useful for conveying accurate information about the concentration of sulfonate groups.

Proton MP Spectra of the Blends. Figure 5a shows the proton multiple-pulse (MP) spectra, using the MREV-8 sequence, for a selection of blends as well as the pure constituents. The spectrum of the initially prepared NC PA looks considerably different from that

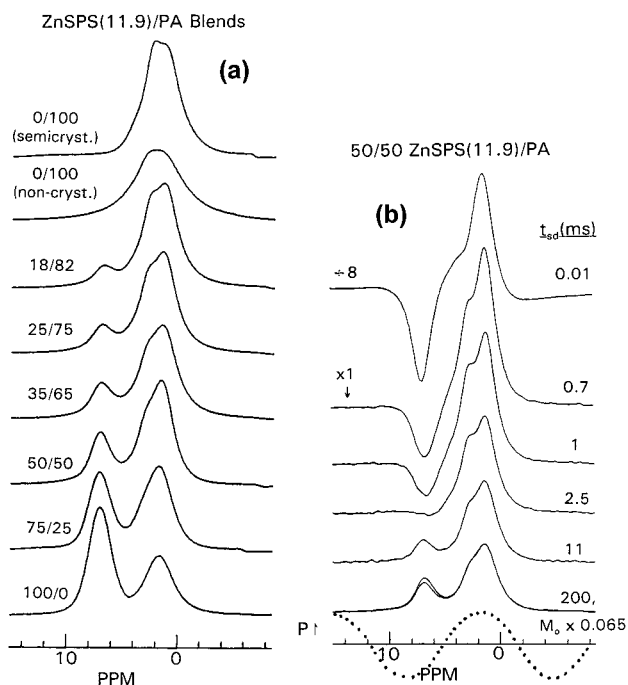


Figure 5. The 200 MHz proton multiple-pulse (MP) spectra of the various indicated ZnSPS(11.9)/PA blends (on left). Spectra are normalized to the same total intensity; aromatic protons resonate near 7 ppm, and aliphatic protons resonate in the 1–4 ppm region. On the right are MP spectra associated with the chemical-shift-based (CSB) spin diffusion experiment applied to the 50/50 ZnSPS(11.9)/PA blend; spin diffusion times are indicated. Vertical amplification factors are also shown along with the sinusoidal variation in the initial polarization. A strong contrast between the aromatic and aliphatic polarizations is initially produced. Much of this gradient dissipates over early times owing to intramolecular spin diffusion. Line shape changes beyond 0.7 ms arise mainly from spin diffusion between the ZnSPS and the PA protons. The M_0 line shape, scaled by 0.065 is superposed on the 200 ms line shape, indicating that spin equilibrium is nearly achieved within this time.

of the semicrystalline PA. Since the PA begins to crystallize a few hours after quenching to ambient temperature, one can obtain a spectrum of a NC PA. This spectrum is broader and more featureless than is the spectrum of the semicrystalline PA. The latter has a narrower and somewhat asymmetric line shape owing to the narrower line shapes associated with resonances of CR protons and the asymmetric distribution of the chemical shifts in the 1.8–3 ppm range. The resonance of the aliphatic protons of PS strongly overlaps with the resonances of crystalline PA. Therefore, while the asymmetric peak shape, accentuating the intensity on the downfield side, is evidence of crystallinity for the pure PA, this asymmetry of the aliphatic proton resonance in the blend spectra becomes weaker evidence for PA crystallinity as the amount of ZnSPS increases. Evident in these spectra is the unique resonance of the aromatic protons of PS at about 7 ppm. This resonance will be used to monitor the proton polarization levels of the PS component in the spin diffusion experiments.

Spin Diffusion Measurements. In general, proton spin diffusion measurements provide some information about the spatial scale over which inhomogeneity occurs in polymers, assuming that one knows the relevant spin diffusion constant(s) which govern the movement of polarization in the presence of polarization gradients. The heterogeneities that can be probed include hetero-

geneities of composition, molecular mobility, and orientation. In the experiments reported here, we emphasize heterogeneities of composition and include a few experiments related to molecular mobility. The generation of an initial polarization gradient that can be understood in terms of composition or mobility is critical to the spin diffusion experiment; moreover, one must be able to monitor the ensuing changes of polarization, arising from spin diffusion, in these same terms. One advantage of spin diffusion experiments that explore compositional heterogeneity is that it is also possible to extract some information about phase composition in a two-phase system.²²

Whether one probes inhomogeneities in composition or mobility depends on the method of preparation of the original polarization gradient. When composition is investigated, a chemical-shift-based (CSB) preparation is used, and the initial polarization profile includes a significant gradient in the average proton polarization associated with each blend constituent. Required is a difference in the MP spectrum of each blend component. When mobility variations are probed, a $T_{1\rho}$ -based preparation is employed, where the initial polarization gradient is based on different relaxation times, i.e., contrasting mobilities, associated with protons at different sites. By allowing $T_{1\rho}$ relaxation to occur for some appropriate period, one can generate an initial polarization rich in those protons with the longer $T_{1\rho}$'s.

1. Chemical-Shift-Based Spin Diffusion Experiments. These CSB spin diffusion experiments will provide information about (a) the intimacy of mixing in mixed regions of PA and ZnSPS, (b) the existence of large domains of substantial compositional difference, (c) the uniformity of composition in the NC regions when PA crystallinity is present, and (d) domain size (in the 4–50 nm range) when domains of substantial compositional difference are present. These experiments will be quite insensitive to the existence of PA crystallinity for those blends where PA is in substantial excess in overall composition.

The pulse sequence for CSB spin diffusion experiment is shown in Figure 6a. This experiment has been described in detail previously,^{21,22} and only a sketch of the concept will be repeated here. This experiment consists of four periods. In the first period, MP methods are used to establish a fixed initial gradient of Zeeman polarization, alternating in sign on consecutive scans. Descriptively, this gradient is simply the MP spectrum multiplied by a sinusoidal function whose phase and period are under the experimenter's control. The choice of phase and period is determined by the MP spectra of the two blend components; the objective is the generation of a strong gradient in the average proton polarization associated with each kind of chain. In the second variable period, t_{sd} , spin diffusion is allowed to take place in the laboratory frame. No rf pulses are applied. In the absence of longitudinal relaxation, T_1^H , the total integral of the signal remains constant during this period, even though the magnetization is redistributing itself in a way which will eventually restore internal spin equilibrium, a state usually distinct from Boltzmann equilibrium. In the third period, one monitors the status of the polarization by taking a MP spectrum, and in the fourth period, one simply waits a time t_0 for the return of Boltzmann-equilibrium polarization. Owing to the quenching of spin diffusion during the application of the MP sequence, spin diffusion is confined to the

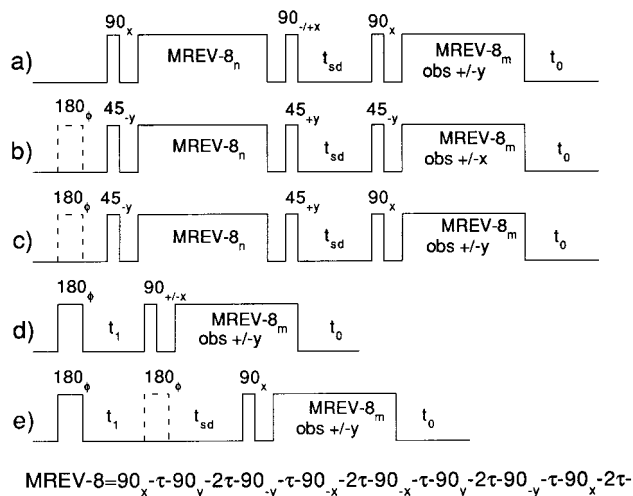


Figure 6. Pulse sequences used in this paper: (a) CSB spin diffusion, (b) $T_{1xz}-T_{1xz}$ spin diffusion, (c) T_{1xz} -MP spin diffusion, (d) inversion-recovery sequence for measuring T_1^H , and (e) T_1^H -selective spin diffusion experiment. Stroboscopic signal observation during the MREV-8 sequence is indicated by the "obs" designation. When a $90_{\pm x}$ precedes the MREV-8 sequence and the detector lies along y , then a MP spectrum is observed; when the prepulse is 45_{-y} and the detector lies along x , then a T_{1xz} decay profile is observed. Dashed-line pulses occur only on alternate scans and " ϕ " designates a phase independently phase cycled over all quadrature values.

second and fourth periods. Its absence from the first and third periods simplifies analysis.

In the experiments reported here, a sinusoidal gradient was produced by applying the MP sequence for observing a MP spectrum^{17,18} for a period of 20 MREV-8 cycles (768 μ s). Considering our experimental scaling ($=0.49$) of the chemical shift under MREV-8, this corresponds to an establishment of a 13.3 ppm sinusoidal period. The choice of rf frequency determines the phase of the sinusoid along the chemical shift axis. The rotor frequency for MAS was chosen (2604 Hz) so that the preparation period is exactly an integral number ($=2$) of rotor periods; this condition eliminates unwanted complications arising from proton chemical shift anisotropy and bulk magnetic susceptibility effects.²¹

The kind of data we obtain is illustrated in Figure 5b for the 50/50 ZnSPS(11.9)/PA blend. The sinusoidal function indicated along the chemical shift scale determines the initial polarization profile. The top spectrum, having a t_{sd} of only 0.01 ms, is essentially that initial profile. That spectrum is displayed with an 8-fold vertical attenuation. The preparation has produced a contrast principally between aromatic and aliphatic protons, and this means that the polarization gradients exist not only between protons on ZnSPS chains and PA chains but also between aliphatic and aromatic protons within each residue of the ZnSPS chains. Since our primary interest is to observe "heteropolymer spin equilibration" and thereby obtain information about the mixing of ZnSPS and PA chains, the process of reequilibration of polarization between protons on the PS chains (and to a lesser extent on the PA chains), i.e., "homopolymer reequilibration", is regarded as uninteresting; however, this latter process does produce considerable change in the spin diffusion line shapes as is evidenced by the 8-fold change in vertical amplification between the two upper spectra. As has been shown by other studies,³³ at a t_{sd} of 0.7 ms, and certainly by 1 ms, the homopolymer spin equilibration is complete;

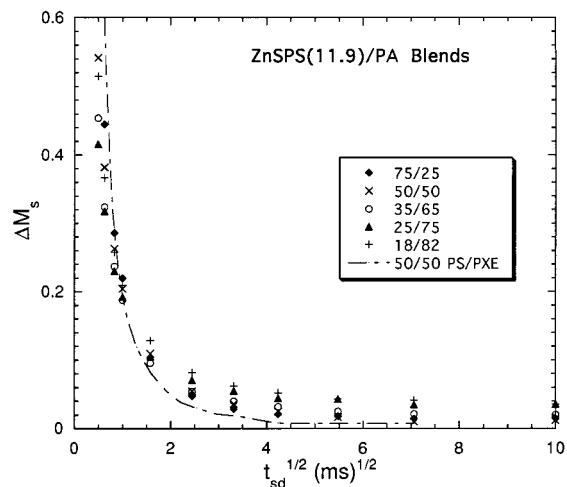


Figure 7. Standardized spin diffusion plots for several blends involving the most decorated ZnSPS(11.9) ionomer. For comparison, data (see ref 33) for the intimately mixed blend of polystyrene and poly(xylylene ether) are included. While PA crystallinity develops in samples where the ZnSPS(11.9) mass fraction is 0.35 or less, these plots indicate that mixing between ZnSPS and PA chains is quite intimate over well-distributed portions of the noncrystalline regions.

hence, in Figure 5b, the development of the line shapes, for $0.7 \text{ ms} \leq t_{sd}$, is dominated by the heteropolymer equilibration which we are interested in. As is illustrated in Figure 5b, the line shapes move toward the Boltzmann-equilibrium (" M_0 ") line shape, i.e., that line shape associated with a uniformly polarized spin population. Thus, in the lower plot the M_0 line shape, scaled by the factor 0.065, is overlaid with the spin diffusion line shape for $t_{sd} = 200$ ms. Note that the line shape change is very minor between $t_{sd} = 11$ and 200 ms; yet, spin equilibrium has not fully been achieved, even after 200 ms, as judged by the slightly greater aromatic intensity of the M_0 line shape. Achievement of internal spin equilibrium is demonstrated when the spin diffusion and M_0 line shapes match since the latter line shape, by definition, arises from the condition of sample-wide spin equilibrium.

In Figure 7, spin diffusion data are plotted for the entire range of blend stoichiometries associated with the most highly decorated ionomer, ZnSPS(11.9). These data are displayed using so-called "standardized" spin diffusion plots,²² in which the abscissa variable is $t_{sd}^{1/2}$ and the ordinate variable, $\Delta M_s(t_{sd})$, is a quantity, proportional to the departure of the ZnSPS proton polarization from internal spin equilibrium. Use of these standardized plots allows comparison of spin diffusion data for different blends and, more importantly, conveniently allows one to make comments about domain stoichiometry in blends.²² The definition of $\Delta M_s(t_{sd})$ for the ZnSPS/PA blends is

$$\Delta M_s(t_{sd}) = [(R_{Ar}(t_{sd}) - R_I(t_{sd})) \exp(t_{sd}/T_1^H)] / [R_{Ar}^{\text{PMSE}}(0) - R_I(0)] \quad (1)$$

where $R_{Ar}(t_{sd})$ is the ratio of the aromatic intensity in the spin diffusion spectrum at t_{sd} to the intensity of that same region in the M_0 spectrum; $R_{Ar}^{\text{PMSE}}(0)$ is that same ratio of aromatic intensity, but corresponding to a sample that is a physical mixture (PM) of the same stoichiometry as the blend, where data are taken under the same experimental conditions of polarization prepa-

ration and where (a) complete spin equilibration (SE) only among the protons of each homopolymer has taken place and (b) T_1^H effects have been accounted for so as to mimic the case where this homopolymer SE happens infinitely fast. $R_{Ar}^{PMSE}(0)$ is the only quantity in eq 1 that requires additional data not available from the spin diffusion data for the blend. One need not use measurements on physical mixtures to generate these data; one can make a series of measurements on the pure blend components instead,²² and this is the approach we took. The other quantity in eq 1, $R_1(t_{sd})$, is the ratio of the total intensity of the spin diffusion spectrum at any t_{sd} to the total intensity in the M_0 spectrum. When internal spin equilibrium is achieved, R_{Ar} and R_1 become equal. The exponential term in eq 1 corrects for T_1^H decay during the spin diffusion experiment provided that spin diffusion leads to full internal spin equilibrium on a time scale short compared to the shortest intrinsic T_1^H 's of each component. This condition prevailed for all but two of our samples, and for those two, corrections for T_1^H were made for the individual components in a more complicated way that was consistent with the separate component T_1^H 's observed in a direct measurement of T_1^H . Reproducibility of all of the $\Delta M_s(t_{sd})$ data, as determined by the difference term in the numerator of eq 1, is typically ± 0.015 , corresponding to 2 standard deviations.

It is apparent that the denominator of eq 1 is merely a scaling factor. This scaling for $\Delta M_s(t_{sd})$ is chosen so that (a) unity represents the asymptote of these data in the absence of spin diffusion between ZnSPS and PA protons, where only homopolymer spin diffusion occurs and goes to completion, and (b) zero represents the achievement of internal spin equilibrium. Hence, when $\Delta M_s(t_{sd})$ values fall below unity, some spin diffusion between ZnSPS and PA protons must have occurred. In Figure 7, only the interval for $\Delta M_s(t_{sd})$ between 0 and 0.6 is shown. In the first millisecond of spin diffusion, $\Delta M_s(t_{sd})$ falls to values near 0.2. This rate of spin diffusion over the first millisecond is very similar to that for the miscible blend of PS and poly(xylylene ether) (PXE).³³ Those data are included in Figure 7 for comparison. However, in contrast to the PS/PXE data, the ZnSPS/PA data fall more slowly with increasing t_{sd} for $t_{sd} > 1$ ms. Moreover, there is a tendency for this last stage of decay to last a little longer as the fraction of PA increases.

From a qualitative point of view, the interpretation of the data of Figure 7 is that a significant amount of intimate mixing is present. Given the spectra of Figure 2, however, where PA crystallinity is evident for those samples having a PA mass fraction ≥ 0.65 , the question arises as to why the spin diffusion plots of Figure 7 do not show more obvious influence from these ostensibly pure domains of PA. The answer to this question is largely one of sensitivity. If one assumes that the blend morphology consists of two phases, one with the NC PA mixed intimately with all of the ZnSPS and a second phase of pure CR PA, the amounts of which phase are given by the f_c^{PA} values in Table 1, then one can calculate that hypothetical value of ΔM_s , namely $\Delta M_s(0)^*$, corresponding to the instantaneous equilibration of all protons in the mixed phase (and no contact between protons in the CR and NC regions). For this case, $\Delta M_s(0)^*$ is given by

$$\Delta M_s(0)^* = f_{PS}^H / [f_c^{PA} - f_{PA}^H] \quad (2)$$

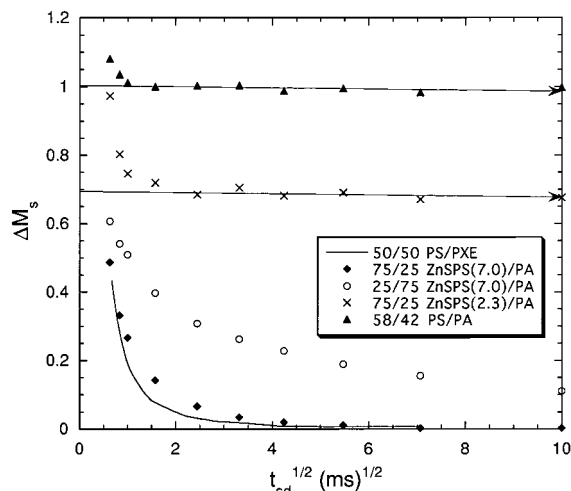


Figure 8. Spin diffusion plots, as in Figure 7, corresponding to blends whose ZnSPS decoration level varies from 7% to 0%. The undecorated, 58/42 PS/PA sample shows no spin diffusion between the PA and the PS ($\Delta M_s = 1.0$), indicating phase separation into large domains of pure components. The 75/25 ZnSPS(2.3)/PA shows an intercept of $\Delta M_s = 0.69$ along with a very shallow slope. The intercept yields stoichiometric information, and the shallow slope indicates large domain size. The 25/75 ZnSPS(7.0)/PA indicates compositional heterogeneity on several distance scales.

where f_{PA}^H and f_{PS}^H are the fractions of the total protons associated respectively with the PA and ZnSPS components. The $\Delta M_s(0)^*$ values corresponding to the semicrystalline samples with 35/65, 25/75, and 18/82 blend stoichiometries are 0.019, 0.024, and 0.029, respectively. These $\Delta M_s(0)^*$ values are very small, which is to say that, given the assumed morphology and given the expectation that spin equilibration within a mixed phase will always be faster than equilibration between phases, the indication that these are semicrystalline samples, as opposed to one-mixed-phase systems, corresponds to differences of less than 0.03 in $\Delta M_s(t_{sd})$ at the longer t_{sd} values. Differences of that order exist between the data for the NC 75/25 and 50/50 samples and the data for the other three semicrystalline samples. That these small differences should be attributed to the presence or absence of crystallinity is a little suspect since those differences persist over rather long spin diffusion times (100 ms), and that would suggest that the domain size for the crystalline regions exceeds several tens of nanometers, which is unlikely, as we show in the section on blends with Cu^{2+} cations.

The principal deduction from Figure 7 is that mixing between the ZnSPS(11.9) and the PA protons, when it occurs, is on a very intimate scale; i.e., homopolymer spin equilibration and most of the heteropolymer equilibration occur on similar time scales. Moreover, these data closely parallel the data for the PS/PXE blend, where it was argued³³ that the average fraction of the available nearest-neighbor sites around any particular residue, which were occupied by heteropolymer residues, was at least as great as that predicted by statistics. Again, a limitation of the data of Figure 7 is its comparative insensitivity to the existence of some minor amount of the dominant blend component existing as a second pure phase, e.g., a crystalline PA phase.

Figure 8 shows standardized spin diffusion plots for other blend samples involving ZnSPS with sulfonate mole fractions less than 11.9%. Again, the PS/PXE reference plot is included. Three of these plots are in

strong contrast to those of Figure 7. First, the physical blend of PS and PA behaves in exactly the manner expected for an incompatible pair of polymers where the domain sizes are so large (> 200 nm) that negligible spin diffusion occurs between domains. As expected, the asymptote of these data occurs at $\Delta M_s = 1.0$, indicating that no detectable spin diffusion has occurred between the PS and PA protons. Given that PS and PA are known to be incompatible from other techniques as well, the asymptote of 1.0 for this case also validates the method of analysis whereby this condition is determined since the definition of ΔM_s automatically implies that one is able, without prior biases, to identify that point where only homopolymer equilibration has occurred.

The data corresponding to the 75/25 ZnSPS(2.3)/PA blend also have an asymptote; however, this asymptote occurs at about $\Delta M_s = 0.69$. The fact that this asymptote is reached in about 4 ms of spin diffusion indicates that mixing, where it occurs, is again on a rather intimate size scale. However, the flatness of the asymptote indicates that there is compositional heterogeneity on a large scale (> 200 nm). We know from Figure 2 and Table 1 that this sample also has some PA crystallinity, but it would be ridiculous to attribute the asymptote to a morphology involving pure-PA crystallites, whose thinnest dimension exceeds 200 nm, surrounded by a mixed phase of uniform composition. Rather, if a pure PA phase, exceeding 200 nm in minimum dimension, were present, this should be a semicrystalline phase with thinner crystallites. It is a characteristic of these spin diffusion curves that there is an ambiguity in the assignment of the phase stoichiometries which give rise to this asymptote.²² Suffice it to say that from these data alone we cannot tell whether this is a two-phase or a three-phase system or whether it is two-phase and one of the phases is a pure phase or whether the pure phase is a PA or a ZnSPS(2.3) phase. However, if the system is two-phase with one pure phase, we can calculate, using an expression analogous to eq 2, what fraction of the PA or of the ZnSPS(2.3) material is associated with this pure phase in order to explain the intercept, $\Delta M_s(0)^* = 0.69$, associated with the asymptote. Respectively, these fractions are 0.764 and 0.877; i.e., the asymptote can be explained, at the extremes, by mixing 23.6% of the PA with all of the ZnSPS(2.3), the mixed phase then having a 93/7 ZnSPS/PA composition, or by mixing 12.3% of the ZnSPS(2.3) with all of the PA, including some small crystallites sprinkled throughout this phase, the mixed phase then having an average 27/73 ZnSPS/PA composition. Of these choices for a two-phase system, the option of a pure PS phase is indicated by looking at the MP line shapes corresponding to the last-to-recover intensity in an inversion–recovery experiment. If one uses difference spectra to look at the last 5%, 2%, and 1% of the recovering magnetization, the line shapes (not shown) converge to that of pure PS. Hence, it is not true that all of the ZnSPS is mixed with a portion of the PA; rather, some portion of the ZnSPS seems isolated from PA.

The 25/75 ZnSPS(7.0)/PA blend data of Figure 8 represent the most complex case and hence the most ambiguous case. There is clearly some mixing on a rather intimate scale, judging by the fast decay to $\Delta M_s(t_{sd}) = 0.6–0.7$. Immediately one can eliminate the idea that this semicrystalline sample consists of PA crystallites ($f_c^{PA} = 0.25$) surrounded by a NC phase of uniform mixed composition. If the latter were true, then

the data should, over the first few milliseconds of spin diffusion, rapidly decay to at least $\Delta M_s = 0.06$, corresponding to equilibration within the NC phase. The experimental decay in the range $1 \text{ ms} < t_{sd} < 40 \text{ ms}$, which should be dominated by interphase spin diffusion, seems to have a significant change in slope near $t_{sd} = 4 \text{ ms}$; values of t_{sd}^* of 4 and 40 ms imply compositional inhomogeneities on distance scales of 8 and 25 nm, respectively. In addition, there is an asymptote at a level of about $\Delta M_s(t_{sd}) = 0.1$ which extends to times of $t_{sd}^{1/2} = 15 \text{ ms}^{1/2}$ (not shown in Figure 8). This longer-time asymptote indicates that there also is some large-scale (> 200 nm) compositional inhomogeneity in this sample. The fact that this asymptote lies above the 0.06 level just mentioned implies that from these data alone one cannot conclude that the PA crystallites are within spin diffusion distance of the ZnSPS; in principle, the PA crystallites might be in a large, separate, semicrystalline PA region. Nevertheless, as will be seen later, the possibility of a separate PA phase is eliminated on the basis of data pertaining to the analogous 25/75 CuSPS(7.0)/PA. The latter data show that all of the PA is within spin diffusion distance of CuSPS regions. In addition, for this ZnSPS(7.0)/PA blend, the MP line shape at the zero-crossing in an inversion–recovery experiment indicates that there is minimal T_1^H dispersion; hence, the possibility that a nearly-pure PS phase is responsible for the asymptote is not supported. Therefore, the asymptote indicates at least two mixed phases of contrasting stoichiometries.

The final sample of Figure 8 is the 75/25 ZnSPS(7.0)/PA blend whose data show a relatively fast equilibration, comparable to the miscible PS/PXE blend. This curve is similar to the data shown in Figure 7. No crystallinity is seen in Figure 2 for this sample, and the long-time asymptote of these data indicates that there is no significant large-scale compositional heterogeneity. The behavior of this decay in the $1–3 \text{ ms}^{1/2}$ range may indicate a slight compositional heterogeneity, primarily on a 10 nm scale.

2. T_{1xz} -Based Spin Diffusion Experiments. These experiments were used to probe the environment around PA crystallites in a few samples that exhibited PA crystallinity. These experiments offered two insights that were not so evident from the CSB spin diffusion data. First, a zone, depleted in ZnSPS concentration, is shown to exist between the PA crystallites and the mixed NC phase. Second, the average repeat distance, which includes the PA crystalline and the mixed NC phases, is estimated.

As previously mentioned, the idea behind these T_{1xz} -based spin diffusion experiments²³ is to obtain information about the domain sizes associated with domains of contrasting molecular mobility. In the ZnSPS/PA blends, the protons in the CR PA domains have the longest T_{1xz} ; hence, in these experiments, the initial polarization profile should have highest polarizations in the CR PA domains.

T_{1xz} is a relaxation time measured during the application of the MREV-8 MP sequence,^{17,18} and it is somewhat analogous to the rotating frame proton relaxation time, $T_{1\rho}^H$, in that molecular motions in the mid-kilohertz frequency range are most effective in bringing about relaxation.^{24,34} T_{1xz} and $T_{1\rho}^H$ stand in contrast to one another in one very important way, namely, that spin diffusion, to a first approximation, is absent during T_{1xz} measurements and present during $T_{1\rho}^H$ measure-

ments. Thus, the polarization gradients which develop during a T_{1xz} decay because of intrinsic differences in molecular motion are expected to be much more localized and spatially sharper using T_{1xz} preparations compared with $T_{1\rho}^H$ preparations. Along with this advantage for T_{1xz} comes the fact that one can obtain an entire T_{1xz} -decay profile in one experiment whereas the $T_{1\rho}^H$ measurement is a point-by-point method. The pulse sequences for the two T_{1xz} -based spin diffusion experiments we employed are given in Figure 6b,c; these vary only in the methods for signal observation. Each starts with a T_{1xz} preparation during which partially decayed magnetization is converted into Zeeman polarization which alternates in sign on consecutive scans. The spin diffusion period is next; then comes the readout period followed by the waiting period where polarization returns to Boltzmann equilibrium. For the "readout" or observation periods, we either obtain T_{1xz} decay profiles (Figure 6b) or MREV-8 spectra (Figure 6c), in each case as a function of t_{sd} . We refer to these experiments respectively as T_{1xz} - T_{1xz} and T_{1xz} -MP experiments.

In concept, these experiments provide two different ways of understanding the spin diffusion following the preparation of the polarization. Given that the preparation has enriched the polarization in those regions with the longest T_{1xz} 's, the T_{1xz} - T_{1xz} experiment will indicate how fast polarization flows to those regions with shorter T_{1xz} 's. On the other hand, the T_{1xz} -MP experiment will provide some complementary compositional information to help interpret the T_{1xz} - T_{1xz} experiment. This compositional information is particularly important for interpreting the results in the blend.

The inclusion of compositional information via the T_{1xz} -MP experiment brings about certain complications arising from the fact that MAS is required in order to provide adequate resolution for distinguishing between the spectra of the two blend components. The problem with MAS is that MAS can create anomalous contributions to T_{1xz} that are not related to molecular motion. Rather than abandoning the method, we choose to select a set of experimental conditions and carefully characterize the initial polarization gradient, even if this gradient arises partially from motional characteristics and partially from anomalous contributions to T_{1xz} . We can then interpret the spin diffusion data in a manner qualitatively correct.

With MAS, as with static samples, pulse imperfections give rise to anomalous contributions to T_{1xz} at the nuclear resonance condition under MP irradiation. Therefore, for static samples T_{1xz} measurements are most reliably performed 3–5 kHz from resonance. For MAS, as opposed to the behavior for static samples, additional anomalous decays occur periodically whenever the rf frequency changes by a multiple of about half the spinning frequency.²² By a suitable choice of rf frequency, these effects can be reduced, but not eliminated. For our experiments we chose the following experimental conditions: MAS frequency = 2604 Hz, MP irradiation time = 35 ms, and rf offset from resonance nominally 3–4 kHz but chosen to maximize the decay rate for a semicrystalline PA sample.

To characterize the initial polarization state in the T_{1xz} - T_{1xz} and T_{1xz} -MP experiments, we conducted several auxiliary experiments using the foregoing experimental parameters. These auxiliary experiments included, for samples of pure PA, pure PS, ZnSPS(11.9), and 75/25 ZnSPS(11.9)/PA, the measurement of T_{1xz}

decays and data from T_{1xz} - T_{1xz} and T_{1xz} -MP sequences with $t_{sd} = 10 \mu\text{s}$. Such data were obtained both non-spinning and spinning. The nonspinning T_{1xz} decays can be relied upon to reflect molecular motion, at least up to T_{1xz} values of about 100 ms. Static-sample T_{1xz} values will represent upper limits for corresponding MAS values. The following information about initial polarization levels, following 35 ms of MP irradiation and relevant to the interpretation of the T_{1xz} - T_{1xz} and T_{1xz} -MP experiments, was gleaned from these auxiliary experiments: (a) NC PA chains that are not mixed with ZnSPS chains have a T_{1xz} , nonspinning, of 2.5–3.0 ms; hence, after 35 ms the initial polarization level in these regions is negligible, whether or not MAS is employed. (b) Nonspinning T_{1xz} 's for the 75/25 ZnSPS(11.9)/PA protons should contain information about the T_{1xz} 's of NC PA chains that are intimately mixed with ZnSPS chains. For this sample, the shortest T_{1xz} component is about 5 ms, not 2.5–3.0 ms. Moreover, the fraction of this faster component in this sample, relative to the faster-relaxing fraction for the pure ZnSPS(11.9) sample, implied that some of the NC PA protons had T_{1xz} 's longer than 5 ms. Therefore, protons on NC PA chains that are intimately mixed with ZnSPS(11.9) chains have their motions, relative to the motions of NC PA chains in a pure PA phase, modified so as to increase T_{1xz} . (c) Under MAS conditions, average initial polarization levels, normalized to Boltzmann polarization levels, lie in the 0.07–0.09 range for PS, ZnSPS(11.9), and 75/25 ZnSPS(11.9)/PA. In addition, for this choice of rf frequency offset, the anomalous contribution to the T_{1xz} decay of aromatic protons is considerably stronger than for aliphatic protons. This results in an initial polarization gradient, between aromatic and aliphatic protons within the PS repeat units, which dissipates over the first, say, 0.7 ms of spin diffusion. (Note that the ability to maintain such an aliphatic/aromatic gradient over 35 ms of T_{1xz} irradiation in pure PS attests to the ability of the MP sequence to quench spin diffusion.) (d) Initial CR PA proton polarization levels are 0.62 of their Boltzmann value (nonspinning) and 0.20 spinning, primarily reflecting a decrease in T_{1xz} from 73 to 25 ms.

In summary, with MAS, the initial polarization profile will be characterized by a polarization level in the PA crystalline region which is 2–3 times larger than the average polarization levels of protons in regions of mixed ZnSPS and NC PA, albeit the aromatic protons in such a mixed region may not exhibit their average polarization until about 0.7 ms of spin diffusion. Any regions of pure NC PA should have negligible proton polarization levels. Note that regions of pure ZnSPS(11.9) are not considered, recognizing that when the ZnSPS(11.9) component is in excess in other blends, no detectable formation of a pure ZnSPS(11.9) phase occurs.

Figures 9 and 10 illustrate respectively the spectral data and the corresponding spin diffusion data obtained from the T_{1xz} - T_{1xz} and T_{1xz} -MP experiments. The sample is an 18/82 ZnSPS(11.9)/PA blend that has been exposed to 100% relative humidity at 45 °C for 30 h and then dried for 3 days in a vacuum at ambient temperature. The reason for the treatment of this "wet-dried" sample was to explore the effect of humidity on the stability of the morphology. PA crystallinity changed from 0.19 to 0.42 as a result of this treatment.

In Figure 9a, the first 40 ms of the " M_0 " T_{1xz} decay is shown. There is a small beating signal at the beginning of the decay associated with the MP spectrum because

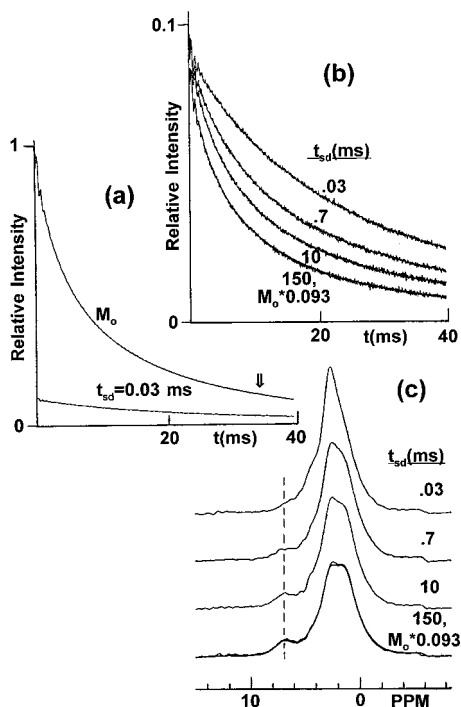


Figure 9. Data associated with T_{1xz} -related spin diffusion experiments performed on the "wet-dried" 18/82 ZnSPS(11.9)/PA blend: (a) Full T_{1xz} decay (M_0) and the decay associated with the $T_{1xz}-T_{1xz}$ experiment at a short (30 μ s) spin diffusion time (t_{sd}); arrow indicates the point at which the magnetization is converted to Zeeman magnetization for the $T_{1xz}-T_{1xz}$ and $T_{1xz}-MP$ spin diffusion experiments. (b) Decays observed for the $T_{1xz}-T_{1xz}$ spin diffusion experiment at various t_{sd} 's where the 150 ms curve is superposed on the scaled M_0 decay to illustrate the similarity of shape. The vertical scale in (b) is amplified 10-fold relative to (a). (c) MP line shapes associated with the $T_{1xz}-MP$ experiment where the gradient preparation and t_{sd} 's are the same as in (b).

the first pulse has not perfectly placed the magnetization in the "spin-locking" direction used to observe the T_{1xz} decay. At the time (35 ms) corresponding to the arrow in Figure 9a, the magnetization is rotated back along the static field, and spin diffusion begins. Also shown in Figure 9a is the decay observed after minimal ($t_{sd} = 30 \mu$ s) spin diffusion has taken place. The initial amplitude of this decay is about 10.3% that of the M_0 decay amplitude, a little lower than the initial amplitude (11.8%) predicted on the basis of 42% of the PA protons assumed crystalline (Table 1) and the remaining material mixed with a polarization level of 0.07. In Figure 9b, a family of $T_{1xz}-T_{1xz}$ spin diffusion curves, including the one for $t_{sd} = 30 \mu$ s, is shown with a 10-fold vertical amplification. One sees the shape evolving back toward the M_0 curve, which is shown scaled by 0.093 and overlaid with the $t_{sd} = 150$ ms curve. The shapes of the latter curves are the same within experimental error, suggesting full internal spin equilibrium at 150 ms.

In Figure 9c, the family of MP spectra, complementary to Figure 9b and corresponding to the $T_{1xz}-MP$ experiment, is shown. Two features about the 30 μ s line shape support the idea that the T_{1xz} preparation has enhanced the polarization in the CR PA regions. First, the intensity of the aromatic PS protons (near the dashed line) is very small, indicating a preferential selection of aliphatic proton magnetization. Second, the aliphatic region has a dominant peak on the downfield side, which peak was associated with PA crystallinity

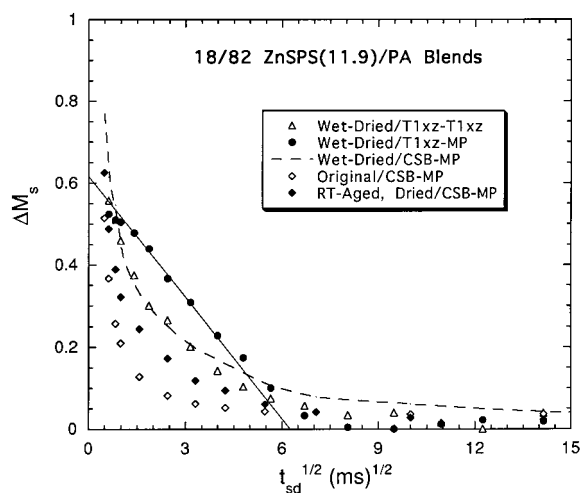


Figure 10. Standardized spin diffusion plots for CSB spin diffusion experiments applied to three indicated preparations of the 18/82 ZnSPS(11.9)/PA blend. See text for details about the aging conditions. It is clear that the "wet-dried" sample has undergone the most extensive separation of components. Also included in the plot are data from the $T_{1xz}-T_{1xz}$ and the $T_{1xz}-MP$ experiments (see Figure 9) on the wet-dried sample. These data are scaled to agree with the CSB datum at $t_{sd} = 0.7$ ms. The $T_{1xz}-MP$ data can be used to deduce an average repeat distance of 20–25 nm as well as a zone of depleted ZnSPS concentration immediately surrounding the PA crystallites.

(see Figure 4). At $t_{sd} = 0.7$ ms, homopolymer equilibration should be largely completed, and intraphase, heteropolymer equilibration in any well-mixed phase should be about 75% complete.³³ At this time the polarization is higher, on average, for PA protons than for the ZnSPS protons; yet, it is also clear that the aromatic region has a nonzero polarization, reinforcing the idea that in the mixed ZnSPS/PA regions the initial average polarization is finite, but less than that in the CR PA regions. By $t_{sd} = 150$ ms, the line shape is close to the M_0 line shape; yet very subtle differences still exist, including a suggestion that the relative CR PA content of the spin diffusion line shape is slightly higher than is found in the M_0 line shape.

Spin diffusion plots for both the $T_{1xz}-T_{1xz}$ and the $T_{1xz}-MP$ experiments are shown in Figure 10 along with three other curves corresponding to CSB spin diffusion experiments. These three curves include the "wet-dried" sample, the original sample that was run 24 h after preparation, and a sample of the original material that was stored in a closed bottle for 14 months. It is clear from inspection of the three latter curves that both the short-term heat/humidity exposure and the longer time aging created substantial changes in the morphology, albeit the extent of the changes was greater in the presence of high humidity. In these plots, the longer time required to reach spin equilibrium means, qualitatively, that mixing of the ZnSPS and PA is no longer as uniform as it was. The increase in PA crystallinity (Table 1) is part of the reason for the change in the shape of the curves. For the wet-dried sample, the CSB data indicate that the morphology is much more complicated than crystallites surrounded by a uniform, mixed NC phase since equilibration within such a uniform phase would predict that $\Delta M_s^* = 0.084$. The fact that the slower equilibration process can be extrapolated back to the ordinate with an intercept approximating $\Delta M_s = 0.4$ implies that the mixing

between the ZnSPS and the NC PA chains is very inhomogeneous (e.g., an intimately mixed phase consisting of all of the ZnSPS and only 28% of the NC PA chains would give $\Delta M_s = 0.4$ after intraphase equilibration). The $T_{1xz}-T_{1xz}$ and T_{1xz} -MP data also present an interesting commentary. But first a word about the choice of vertical scaling for these latter plots.

These T_{1xz} data cannot be scaled in the way the CSB data could be since the initial polarization profile for the T_{1xz} data is understood in only qualitative terms. Thus, the quantities plotted are simply the T_1^H -corrected deviations from the scaled M_0 line shapes of (a) the faster-decaying component of the T_{1xz} decay in the $T_{1xz}-T_{1xz}$ experiment and (b) the aromatic signal in the T_{1xz} -MP spectrum. Thus, both sets of spin diffusion data are arbitrarily scaled to coincide with the $t_{sd} = 0.7$ ms point in the CSB curve for the "wet-dried" sample. At the same time, $\Delta M_s(t_{sd}) = 0$ retains its meaning as the achievement of internal spin equilibrium.

The T_{1xz} data of Figure 10 offer three insights in the range $t_{sd} \geq 1$ ms, where changes are dominated by interphase spin equilibration, given that the initial polarization is greatest for the protons in the CR PA regions. First, in all three sets of spin diffusion data for the wet-dried sample, but most clearly for the T_{1xz} -MP data, one can see a roughly linear portion of the decay whose slope would have an intercept with the abscissa near $6 \text{ ms}^{1/2}$. Such an intercept can be associated with a morphology whose overall repeat distance is in the 20–25 nm range;²² i.e., this would be the minimum length over which the average composition would be expressed, and it is also the distance corresponding to the sum of the average minimum domain dimensions of the phases. Second, the $T_{1xz}-T_{1xz}$ data show that in the range from $t_{sd} = 1$ to 2 ms considerable polarization is moving from the slower to the faster relaxing protons. Third, during this same t_{sd} period, very little change is occurring in the PS intensity in the T_{1xz} -MP experiment, although the initial conditions in the $T_{1xz}-T_{1xz}$ and T_{1xz} -MP experiments are identical.

The latter two observations together are interpreted in terms of a region, between the CR PA and the mixed phase which looks more like pure, NC PA in the sense that when magnetization diffuses into this region, primarily from the protons in the PA crystals, the fraction of protons with short T_{1xz} 's sharply increases, but the aromatic proton polarization of PS hardly changes. The "bending over" of an interphase equilibration curve as t_{sd} approaches zero is indicative of a finite interface of compositional change in CSB spin diffusion plots;²² a similar qualitative argument can be made here. The time scale ($0.7 \leq t_{sd} \leq 40$ ms), along with our knowledge of the initial polarizations, dictates that the process observed via the T_{1xz} -MP data over this time scale is mainly spin equilibration (though not necessarily complete equilibration) between CR PA protons and PS protons in the mixed phase. The bending over of the data reflects the fact that the polarization of the CR PA protons does not diffuse immediately to the PS protons in the mixed phase as it would if the mixed phase had a uniform ZnSPS/PA stoichiometry and formed the immediate boundary around the PA crystallites (recall this simple two-phase morphology was also rejected on the basis of the CSB data). The thickness of this interface region is harder to estimate since estimation of this thickness demands that one know the average initial polarization of this interfacial region as well as

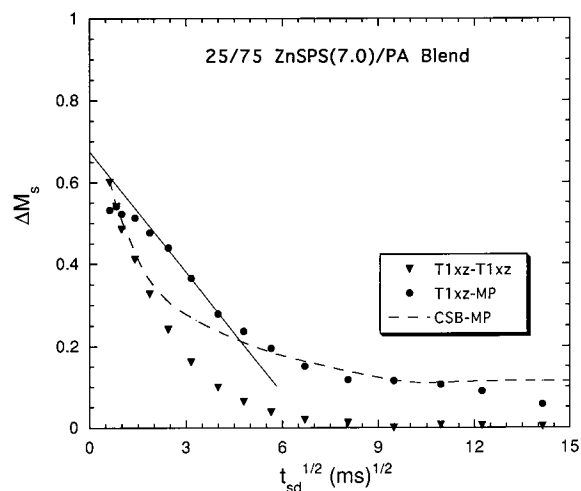


Figure 11. Spin diffusion plots such as those of Figure 10 for the 25/75 ZnSPS(7.0)/PA blend. Again, the 20–25 nm repeat and the zone of depleted ZnSPS concentration surrounding the PA crystallites are evident.

the change in PS concentration with distance from the PA crystallites.

Figure 11 compares these three kinds of spin diffusion data for the original 25/75 ZnSPS(7.0)/PA sample. The CSB data for this sample show an asymptote at longer times which indicates some compositional heterogeneity on a larger (>200 nm) size scale. The $T_{1xz}-T_{1xz}$ data again show brisk spin diffusion between protons with longer and shorter T_{1xz} 's in the 1–2 ms range, and again, the T_{1xz} -MP data support the notion of a zone, depleted in ZnSPS concentration, immediately surrounding the PA crystals. Also, these latter data give evidence for an overall periodicity in the 20–25 nm range. Interestingly, however, of the two T_{1xz} -type spin diffusion experiments, only the T_{1xz} -MP spectrum shows the large-scale compositional inhomogeneity. It is within the realm of possibility that the $T_{1xz}-T_{1xz}$ data do not show this given that the criterion for coming to equilibrium in the $T_{1xz}-T_{1xz}$ experiment depends on duplicating the sample-wide mix of relaxation times and not the sample-wide composition within spin diffusion distances from the PA crystals. In principle, it is possible, although not so probable, that the mix of relaxation times for the material surrounding and including the PA crystals could look like the sample-average mix even though the average composition of that material is not the sample-average composition.

Finally, we also conducted both the T_{1xz} -MP and $T_{1xz}-T_{1xz}$ experiments on the original 18/82 ZnSPS(11.9)/PA blend and just the T_{1xz} -MP experiment on the semicrystalline 25/75 ZnSPS(11.9)/PA blend and obtained results (not shown) similar to those given in Figures 9 and 10; i.e., in the T_{1xz} -MP experiment, there was a bending over of the data at short t_{sd} values, and the slope of the data gave a t_{sd}^* in the 30 nm to 35 ms range, implying overall repeat distances in the range of 18–25 nm.

Thus, these semicrystalline samples seem to be characterized by PA crystalline phases, surrounded by a PA-rich, NC interface, which, in turn, resolves into a mixed ZnSPS/PA phase, the overall repeat distance, on average, being 18–25 nm. In addition, there is some large-scale (>200 nm) compositional inhomogeneity which varies from sample to sample but which seems

to gain prominence as the decoration level of the ZnSPS component is reduced. While the latter trends in large-scale inhomogeneity were evident already in the CSB experiments, the T_{1xz} - T_{1xz} and T_{1xz} -MP experiments together yielded a much better estimate of the overall repeat distance and established the existence of the interface region. Some summary designations regarding the morphology of the Zn-containing ionomers and blends are included in Table 1.

T_1^H Measurements. Observation of MREV-8 spectra as the readout method for monitoring recovering magnetization in a T_1^H experiment (see Figure 6d) allowed us to determine T_1^H from the t_{1z} values, i.e., the t_1 's at the "zero crossings" where the initially inverted signal changed from negative to positive. ($T_1^H = t_{1z}/(\ln 2)$) for a fully inverted initial magnetization and a single T_1^H ; the typical inversion level in our experiments was $-0.97M_0$.) Performing the T_1^H measurement in this way also allowed us to monitor the line shape near the zero crossing, and by being able to distinguish the ZnSPS signals from the PA signals, we could tell whether the ZnSPS and PA protons had the same or different spin-diffusion-averaged, sample-averaged T_1^H 's. When these T_1^H 's are the same, there is a complete null at the zero crossing, and when these T_1^H 's differ, relatively, by as little as 5% different, the signal level of one component is still 3% of its Boltzmann-equilibrium amplitude when the other signal is passing through zero; hence, relative differences in T_1^H 's of the order 5% or more can usually be detected on the basis of the line shapes in the vicinity of the zero crossings. To see such differences in T_1^H 's, one must satisfy three conditions: (a) the intrinsic T_1^H 's, averaged over all occupied sites, for the protons of each blend phase must differ, relatively, by at least 5%, (b) the composition of each phase must be sufficiently different so that the spectra of each phase will have significant contrast, and (c) the effective averaging of different T_1^H 's, owing to spin diffusion, must not occur. Whether spin diffusion equalizes unequal intrinsic T_1^H 's is partly a question of the values of those intrinsic T_1^H 's, partly a question of whether there is a lot of motional averaging and a slowing down of spin diffusion in one or both of the phases, and partly a question of the domain sizes. Crudely, in the ZnSPS/PA blend system, where component T_1^H 's ranged from about 0.6 to 1.6 s and where large-amplitude motional averaging is modest to nonexistent, as judged by the proton Bloch-decay line shapes, one would require, according to model calculations, domain sizes of the order of 20 nm (or overall repeat distances of about 40 nm) in order to see T_1^H effects at the zero crossing supposing that T_1^H 's had the maximum disparity. However, considering that most of these samples have some region of mixing, the T_1^H 's and line shapes associated with each phase will become less disparate; hence, one would likely need domain sizes larger than 30 nm in order to observe line shape effects at the zero crossing. Given this perspective, the only ZnSPS/PA blends that showed clear line shape anomalies at the zero crossings were the 58/42 PS/PA and the 75/25 ZnSPS(2.3)/PA blends, both of which, according to Figure 8, had very large domains. In the latter sample, if one has a pure and a mixed phase coexisting, the average T_1^H 's given in Table 1 are more consistent with the ZnSPS, rather than the PA, comprising the pure phase. Of note is the fact that the line shapes at the zero crossing showed no disparate T_1^H 's for the 25/75 ZnSPS(7.0)/PA blend, even though the spin

diffusion plot suggested some larger-scale compositional heterogeneity.

There is a second perspective pertaining to the T_1^H data of Table 1. The primary reasons for taking the T_1^H data were to set the appropriate pulse repetition times for the spin diffusion measurements, to correct for T_1^H effects in the spin diffusion data analysis and to look for evidence of large-scale phase separation. We were less interested in interpreting trends in the T_1^H data. Thus, even though the samples were vacuum-dried, there may be a slight contribution from small variations in residual water and from paramagnetic oxygen. We made no attempt to exclude the latter from the samples; moreover, the sample-spinning gas was air, not nitrogen. The plastic end caps on the sample rotors act as seals, but they are not airtight.

Keeping in mind the foregoing caveats, we will still make a few observations along with some tentative interpretations. In the pure ZnSPS materials, it is intriguing to see the decrease in T_1^H as the level of sulfonation increases (even though this decrease in T_1^H is not monotonic—a trend that was rechecked). This trend in T_1^H may imply that up to a certain level the tendency of the polar moieties in ZnSPS to aggregate³⁵ makes the packing of chains less efficient so as to promote local, anisotropic mobility; however, at higher levels of sulfonation, the net effect of the increasing concentration of associating sites is to restrict chain movement. (On the basis of the Bloch-decay spectra of these pure ZnSPS materials, different levels of residual water cannot explain these T_1^H 's.) Note that for the 75/25 blends the trend in T_1^H seen for the pure materials is preserved; i.e., T_1^H is shorter when the ZnSPS(7.0) component is present than when ZnSPS(11.9) is involved. For the 25/75 blends, the trend is reversed ostensibly because there is greater PA crystallinity in 25/75 ZnSPS(7.0)/PA relative to 25/75 ZnSPS(11.9)/PA. (For the pure PA, the presence of crystallinity causes a significant increase in T_1^H , owing to the diminished mobility of the crystalline chains.)

Experiments Using Paramagnetic Copper. Motivations for substituting Cu^{2+} for Zn^{2+} and studying the influence of this paramagnetic ion on the behavior of the protons included the following considerations: (a) Cu^{2+} and Zn^{2+} have similar size and the same valence; moreover, IR studies show them to form complexes with PA with similar strength.^{36,37} Therefore, the morphologies of the Cu and Zn blends are expected to be similar, and one could possibly resolve certain areas of morphological ambiguity in the ZnSPS/PA blends by studying the analogous CuSPS/PA blends. (b) Cu^{2+} has a single unpaired electron which, on the basis of some general considerations³⁸ and an inspection of the published³⁶ ESR spectra (taken at 77 K) of certain of these Cu-containing blends, is expected to have a longitudinal relaxation time, T_1^e , in the approximate vicinity of the proton Larmor period.³⁸ The dipolar coupling of proton spins to these rapidly relaxing, unpaired electrons is expected to offer a significant contribution, if not dominate, the T_1^H of nearby protons. This direct relaxation mechanism, neglecting angular dependence, is short-range, having a dependence on the inverse sixth power of the electron–nuclear distance.^{25,39} Importantly, all other protons within distances accessible by spin diffusion²² will also have their relaxation times affected. Thus, changes in proton relaxation, relative to the analogous, diamagnetic Zn-containing materials, would

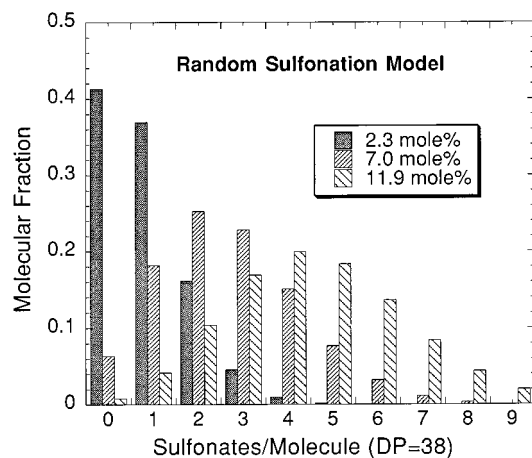


Figure 12. Histograms, for the three SPS materials used, showing the statistical distribution of molecular fraction versus the number of sulfonate groups per PS molecule assuming random sulfonation and a DP of 38.

indicate proximity to metal ions. (c) If the influence of the Cu ions on proton relaxation is sufficiently great, then one might test whether large domains (> 100 nm) of pure PA (or undecorated PS) exist in any of the blend samples. One would simply look for protons that have long T_1^H 's typical of pure PA or undecorated PS; one could also isolate the MP spectrum of the longer relaxing components to help verify the claim. (d) There is considerable interest in the homogeneity of the distribution of ions in ionomers.^{40–42} Generally, the X-ray scattering patterns of pure ionomers contain small-angle scattering as well as a weaker peak^{35,40} corresponding to a spacing of ≈ 3 – 4 nm. We wanted to distinguish whether this latter periodicity is indicative of the radius of or the spacing between aggregates of ions. Moreover, the origin of the small-angle intensity is poorly understood beyond a consensus that the scattering is related to the ions. In particular, it has been postulated that the distribution of ions is inhomogeneous on a length scale from "nanometers to microns".⁴² Hence, it seemed natural to investigate the homogeneity of relaxation in the pure CuSPS ionomers in the hopes that something about the homogeneity of the ion distribution would be revealed. Since the DP of our average SPS molecule is rather small (≈ 38) and since the sulfonation is assumed to be random, there should be a substantial distribution in the number, S_i , of sulfonate groups per molecule, where i refers to the i th molecule. Figure 12 is a histogram showing the statistical fraction of molecules corresponding to each possible S_i value between 0 and 9. The values in Figure 12 for each ZnSPS material are based on assumptions of random sulfonation and a DP of exactly 38. Note the nontrivial fractions that are undecorated for the CuSPS(2.3) and the CuSPS(7.0). One distinct possibility in these samples is that there will be some inhomogeneity in the Cu distribution based on a spatial partitioning of molecules according to their S_i values. This partitioning might give rise to the increase in intensity at low angles observed by SAXS. Large domains of undecorated chains ($S_i = 0$) should be evidenced by long T_1^H 's; we particularly looked for such domains in the CuSPS(2.3) sample.

1. Focus of the Experiments and Discussion.

Several samples containing Cu were studied. These included the pure ionomers, CuSPS(11.9), CuSPS(7.0), and CuSPS(2.3), along with selected blends. Because the influence on T_1^H resulting from the unpaired Cu elec-

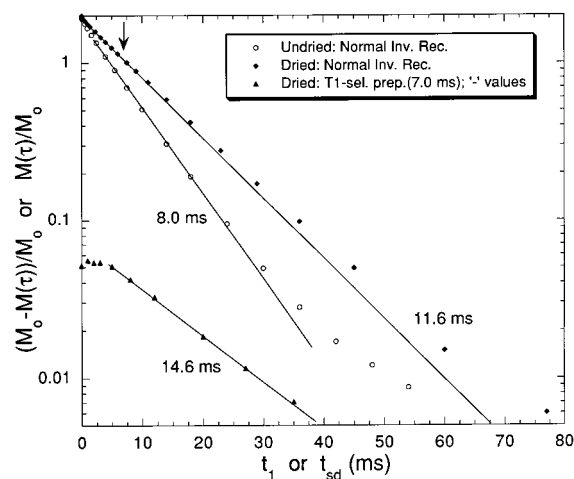


Figure 13. Proton inversion–recovery data for paramagnetic CuSPS(11.9) in its dried and undried states. Data (shown positive whereas data are actually negative) for the T_1^H -selective spin diffusion experiment of Figure 6e are also given. The straight lines are drawn to capture the slopes for those points exceeding 4 ms. The reasonable agreement between the 11.6 and 14.6 ms time constants indicates that the dispersion in T_1^H is not very large for this material. More than 95% of the protons are included in these data.

trons turned out to be rather complicated, we limit ourselves to a detailed discussion of only two samples and indicate the principal question addressed in each of these samples. Data for other samples will be presented but will be discussed only qualitatively in the context of discussions about the two primary samples.

The samples and associated questions are these: First, for the pure ionomer, CuSPS(11.9), can we extract information about the concentration fluctuations of Cu sites on a distance scale a few times larger than the average spacing between Cu sites? We do this by analyzing for the distribution of average T_1^H 's associated with domains of such size. A knowledge of the dependence of T_1^H on the mole fraction of Cu is critical for converting any T_1^H distribution to fluctuations in Cu concentration. Data for other Cu ionomers and blends help to establish this dependence.

Second, for the 75/25 CuSPS(2.3)/PA blend we look for evidence that the CuSPS chains in the mixed phase have a higher-than-average concentration of decorations (Cu sites) and that the unmixed (or poorly mixed) phase has lower-than-average decoration levels. This expectation seems reasonable since (a) the suppression of PA crystallinity, as a measure of chain mixing, is highly correlated with the overall density of decorations and (b) spin diffusion behavior also shows that there is better mixing at a given blend stoichiometry when the MSPS decoration level is higher. The foregoing arguments point to more favorable energetics of mixing for more decorated chains, but one cannot, on this basis alone, forecast a definite partitioning of the MSPS chains based on decoration level; we seek direct evidence using this Cu-containing blend.

2. T_1^H Distribution in CuSPS(11.9). Figure 13 includes data from an inversion–recovery experiment (see Figure 6d) with MP readout for dried and undried samples of CuSPS(11.9), the latter having been in a closed bottle in the laboratory for 2 months. The amount of water picked up by this sample is not known. The inversion–recovery data are characterized by small departures from exponentiality over the first few mil-

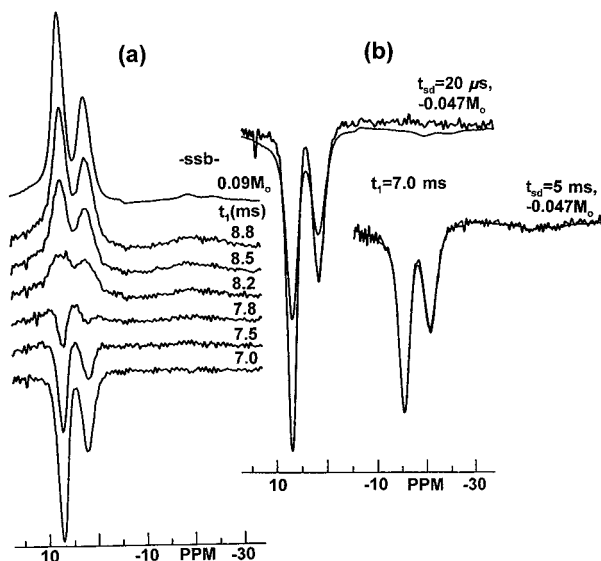


Figure 14. MP line shapes associated with the dried CuSPS(11.9) in the inversion-recovery (a) and the T_1^H -selective ($t_1 = 7$ ms) spin diffusion experiments (b). (a) illustrates that broader line shape features recover faster, as does the average intensity of the first spinning sideband (ssb). This is also illustrated in (b) where a scaled M_0 spectrum is compared at $t_{sd} = 20 \mu\text{s}$. Comparison at $t_{sd} = 5$ ms shows that the rapidly relaxing spins near the Cu^{2+} sites are strongly coupled by spin diffusion to the remaining spins.

liseconds and also by a modest departure from exponentiality at longer times. The lines drawn are linear extrapolations of the slopes starting at $t_1 = 4$ ms; they yield average T_1^H 's of 8.0 and 11.6 ms for the undried and dried samples, respectively. Compared to the 928 ms T_1^H of dry ZnSPS(11.9) (Table 1), the T_1^H 's of the CuSPS(11.9) are about 2 orders of magnitude shorter. Hence, as was hoped, the T_1^H of CuSPS(11.9) is dominated by the paramagnetic contribution to relaxation. The nonexponentiality at short times is presumably associated with the process of establishing steady-state polarization gradients over distances typical of the separation between paramagnetic centers; deviations at longer times reflect inhomogeneities in average T_1^H 's over larger distances. Selected spectra corresponding to the dried sample in the vicinity of the zero crossing are shown in Figure 14a as a function of t_1 . Two expected points can be confirmed qualitatively in these spectra, namely, (a) the faster relaxing component has the broader line shape and (b) the intensity per spin at the first spinning sideband, shown on the upfield half of the spectrum, is greater for the broader component. These features are expected when those proton spins closer to the Cu sites experience stronger interactions with the electron moments, both in the intensity of the fluctuating dipolar field for producing relaxation and in the strength of the averaged, nonvanishing dipolar coupling to the electron. (Even though MAS tends to average this latter coupling to zero, stronger spinning sidebands result.)

Also shown in Figure 13 are the data from a T_1^H -selective experiment (see Figure 6e) for the dried sample where the initial magnetization profile is captured at the point of the arrow in Figure 13 and corresponds to the spectrum at $t_1 = 7.0$ ms in Figure 14a. In principle, this is a spin diffusion experiment, but because of the short T_1^H 's which characterize this sample, the data after 5 ms are dominated by T_1^H decay. From the longer-time behavior this experiment yields an apparent T_1^H

of 14.6 ms, somewhat longer than the 11.6 ms average. In concept, this experiment weights, with increasing strength, those T_1^H components that deviate more strongly from a T_1^H of 10.1 ms; the latter components are nulled at $t_1 = 7$ ms. Qualitatively, if there were components, even though minor components, with T_1^H 's much longer than 10 ms, they would have a much stronger relative influence on the decay in this T_1^H -selective experiment relative to the normal inversion-recovery experiment. Also, because T_1^H components shorter than 10 ms make an initial positive contribution to the signal while those components with T_1^H 's longer than 10 ms give a negative contribution, a wider range of T_1^H 's will show up as a more strongly nonexponential plot compared with the inversion-recovery data. The fact that the T_1^H -selective data are characterized both by an increase in average T_1^H of only 26% over the overall mean T_1^H and by a nearly exponential behavior over a decade of decay implies that only a modest distribution of T_1^H exists.

Figure 14b shows two T_1^H -selective spectra at $t_{sd} = 0.05$ and 5 ms, corresponding to the early and later stages in the establishment of the steady-state proton-polarization gradients between paramagnetic centers. Each spectrum is also superposed on the M_0 spectrum, scaled down by the factor -0.047 . This scaling makes the integrals the same for each pair of spectra and, at the same time, allows for a normalized line shape comparison. At 0.05 ms, the intensity of the narrower spectral features arising from those spins further from paramagnetic sites is more negative than in the M_0 spectra, while the broader features, including the upper spinning sideband, are slightly positive. At 5 ms, the T_1^H -selective line shape reflects a polarization distribution which includes the steady-state polarization gradient between paramagnetic centers. The fact that this line shape and the M_0 line shape are very close indicates that, on a 5 ms time scale, spin diffusion coupling between the faster- and slower-relaxing spins is quite strong.

To extract a reasonable estimate of the distribution in T_1^H from the data of Figure 13 for the dry sample, we conducted our analysis within the following two guidelines. The first guideline was that we would ignore the first 4 ms of data, recognizing (see Figures 13 and 14b) that this was the period of time necessary for establishing, via spin relaxation and spin diffusion, steady-state proton polarization gradients over typical distances between paramagnetic centers. In other words, we would not try to mimic spin diffusion over these short distances. The second guideline stemmed from the recognition that fitting data to sums of exponentials is a very imprecise activity when the time constants are within a factor of 2 or 3. Hence, while we did fit the data to a two-exponential model, similarly good fits could be obtained using a substantial range of relative amplitudes and time constants. Therefore, we also decided to use a one-parameter model having a Gaussian distribution of relaxation rates (rate = $(T_1^H)^{-1}$) where the mean rate was fixed at $(11.6 \text{ ms})^{-1}$. The results of simultaneously fitting both the inversion-recovery and the T_1^H -selective data to the same two-exponential (selected) or Gaussian distribution are given in Figure 15. For these fits, no spin diffusion is assumed between regions of different T_1^H .

In Figure 15, the particular two-exponential fit chosen is made up of a 92% contribution with a T_1^H of 11.25

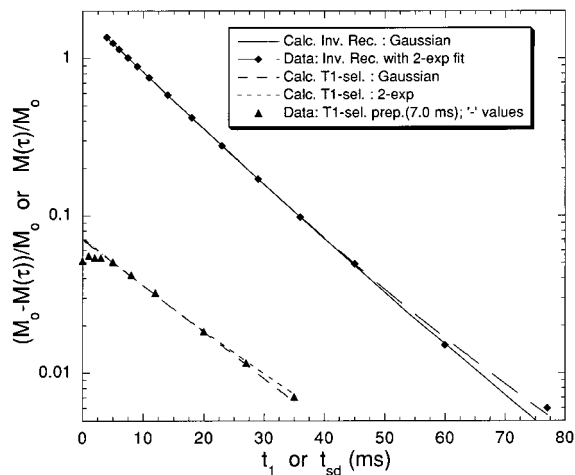


Figure 15. Calculated fits to the T_1^H data and the T_1^H -selective spin diffusion data of Figure 13. The Gaussian fit is a single-parameter fit to a Gaussian distribution of relaxation rates, assuming that the mean T_1^H is known. The two-exponential fit is one of many acceptable fits; however, it represents a fit where both the amplitudes and the T_1^H are disparate. See text for further details.

ms and an 8% contribution with a T_1^H of 20.28 ms. This fit represents a variation in T_1^H of about a factor of 2 when the amplitudes are quite disparate. Fits with more comparable amplitudes are also reasonable; in fact, for equal amplitudes, the disparity in T_1^H 's is a factor of about 1.5. The Gaussian, single-parameter fit, using a fixed mean rate of $(11.6 \text{ ms})^{-1}$, gives a half-width at half-height for the Gaussian distribution of 0.0157 ms^{-1} . The corresponding T_1^H range for one standard deviation ($\approx 68\%$ of the population) is 10.1–13.8 ms and for two standard deviations ($\approx 95\%$ of the population) is 8.9–16.9 ms, i.e., less than a factor of 2 in T_1^H .

The analysis just offered did not take account of spin diffusion beyond the approximate way short-range spin diffusion between paramagnetic centers was accounted for. Spin diffusion occurring on a larger scale would have the effect of reducing the range of T_1^H 's. Hence, we attempted to estimate the domain size to be averaged over to obtain T_1^H 's with this width of distribution. We did this by modeling spin diffusion in a simple, 1-D lamellar morphology (with equal mass fractions) where two alternating regions, having different T_1^H 's, were assumed. The T_1^H 's were chosen on the basis of a two-exponential fit of the experimental data using the constraint of equal mass fractions. Then the relaxation profiles were calculated, including diffusion, and the output was again fit to the sum of two equal-amplitude exponentials. The ratio of the two T_1^H 's obtained from this fit, relative to the ratio of the original T_1^H 's, was used as a measure of the influence of diffusion as the domain size was varied. On the basis of this calculation, we make the following statement about the distribution of T_1^H 's in the dry CuSPS(11.9) sample: 95% of the average T_1^H 's, averaged over a domain size of 14 nm, lie within a factor of 1.4 compared to the mean T_1^H of 11.6 ms. In other words, the total range of T_1^H for these 95% of domains is a factor of 2.

We note in passing that the time interval of 4–5 ms which is required for the establishment of the steady-state polarization profiles (see Figures 13 and 14b) could, in principle, be used to estimate an upper limit on the distance scale or periodicity in the ZnSPS(11.9) ionomer. The 4–5 ms range would represent an upper

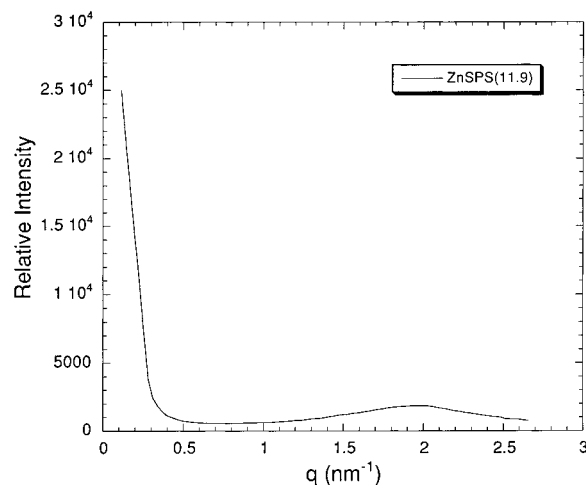


Figure 16. Small-angle X-ray scattering pattern of the ZnSPS(11.9) ionomer. The scattering maximum at 1.96 nm^{-1} corresponds to a 3.2 nm periodicity. The increase in intensity at low angles is typical of ionomers.

limit because the time required for full equilibration from spin diffusion exceeds the characteristic times usually used to extract domain dimensions (see, for example, in Figure 10 that the intercept of the extended slope corresponds to a t_{sd} of about 40 ms and the time for more complete equilibration is closer to 70 ms.) Times of 4 and 5 ms correspond respectively to distances of 1.8 and 2.0 nm if we use a spin diffusion constant^{22,43} of $0.6 \text{ nm}^2/\text{ms}$, and the formula,²³ $\langle x^2 \rangle = 4Dt/3$, for relating the rms distance that a diffusion front travels along one dimension in a given time. Experimentally, we have looked for periodicity using small-angle X-ray scattering; the scattering pattern for the ZnSPS(11.9) ionomer is shown in Figure 16. There is a rather broad peak at a q of 1.96 nm^{-1} corresponding to a periodicity of 3.2 nm, i.e., just under twice the distances just estimated. It is fairly typical^{35,40} for these ionomers to show a peak in the 3–4 nm range, and there is a question whether this peak represents the spacing between aggregates of ions or whether this peak relates to the size of the ionic clusters themselves. On the basis of the 4–5 ms equilibration time, we cannot directly comment on which of these possibilities is preferred. Suffice it to say that the observed equilibration time is certainly consistent^{22,43} with an overall periodicity of 3.2 nm, where 3.2 nm represents the average separation between clusters. If one invoked the alternate idea that 3.2 nm represented the diameter of clusters, then the density of decorations within a given chain and the mean separation (about eight repeat units) between sulfonate decorations would imply that the clusters were not very dense in the metal-sulfonate groups. Moreover, the mean distance between such large clusters would have to be no more than about 6 nm^{22,43} in order to satisfy the equilibration times. A mean distance of 6 nm, however, would imply that a significant fraction of metal-sulfonate groups would be found outside of the 3.2 nm clusters. It seems more plausible to us that the 3.2 nm scattering maximum corresponds to the distance between smaller ionic clusters. Then the geometry is right for incorporating most of the metal-sulfonate groups within each cluster. Also, since, from Table 2, nonaggregated Cu atoms have an average spacing of 1.44 nm, aggregates spaced at 3.2 nm would then contain about 10 Cu ions per aggregate, assuming that all Cu atoms participate in clusters.

Table 2. Observed Proton Relaxation Times (T_1^H), Inferred Proton Relaxation Times Associated with the Presence of Paramagnetic Cu (T_{1p}^H), Theoretical Cu–Cu Distances (r_{Cu-Cu}), Assuming a Uniform, Simple-Cubic-Lattice Distribution, Relative Proton Relaxation Efficiencies (RPRE) per Cu Ion, Referenced to the Dry CuSPS(11.9) Material, and Deductions Pertaining to or Based on Each Sample

sample	T_1^H (ms) ^{a,d}	T_{1p}^H (ms) ^{b,d}	r_{Cu-Cu} (nm)	RPRE ^d	deductions
CuSPS(11.9)-dry	11.6(3)	11.7(3)	1.44	1.00 (def)	range of C_{Cu} , averaged over 14 nm, below factor of 1.30
CuSPS(11.9)-undried	8.0(3)	8.1(3)	1.44	1.45(10)	water changes T_1^e
CuSPS(7.0)-dry	68(3)	76(4)	1.70	0.26(4)	chains with differing S_i show little segregation
CuSPS(2.3)-dry	930(30)	2700(400)	2.41	0.022(4)	chains with differing S_i show little segregation
CuSPS(2.3)-dry-ann. at 170 °C	640(20)		2.41		aggregates grow with annealing
20/80 CuSPS(11.9)/PA-dry	38.5(20)	40.0(23)	2.46	1.17(8)	no evidence of large, pure-PA phase
25/75 CuSPS(7.0)/PA-dry	65(3)	71(4)	2.70	1.46(15)	introduction of PA increases RPRE
75/25 CuSPS(2.3)/PA-dry ^c	200(15)	270(25)	3.73 (2.65 av)	1.14(13)	higher-than-average concentration of Cu in mixed phase ambiguous (not confirmed)
75/25 CuSPS(2.3)/PA-dry-ann at 130 °C ^c	≈200(15)		3.73 (2.65 av)		aggregates grow with annealing

^a (T_1^H) values are based on the initial slope of the decay curves. ^b (T_{1p}^H)⁻¹ is defined in eq 3. ^c Applies to the mixed, semicrystalline phase only where that phase contains all of the PA and 12% (assumed) of the CuSPS(2.3); no partitioning of CuSPS(2.3) chains according to decoration level is assumed in computing RPRE. (The average r_{Cu-Cu} would be 2.65 nm if this sample consisted of a single, uniformly mixed phase.) ^d Estimates of the expanded uncertainty appear in parentheses and are given in units of the last decimal place.

3. Measurements Pertaining to the Interpretation of T_1^H in Terms of Cu Concentration. The foregoing section established a distribution of T_1^H 's in the ionomer, CuSPS(11.9). We really wish to probe the distribution of Cu concentration, C_{Cu} . Some relationship between T_1^H and C_{Cu} is, therefore, needed. Actually, we should try to establish a relationship between T_{1p}^H and C_{Cu} where T_{1p}^H is the paramagnetic contribution to T_1^H , approximated by the formula

$$(T_{1p}^H)^{-1} = [T_1^H(Cu)]^{-1} - [T_1^H(Zn)]^{-1} \quad (3)$$

where the latter quantities refer to the measured T_1^H 's for the analogous Cu and Zn ionomers or blends. What follows here should be regarded as a semiquantitative approach to this problem.

Given that the Cu ions have a tendency to aggregate,³⁵ it is conceivable that the electron relaxation time, T_1^e , would vary according to the state of aggregation. Also, in the blends, it is conceivable that T_1^e will change according to whether an amide moiety interacts with the Cu. Since the influence of the Cu on T_{1p}^H depends both on the distribution of protons around the Cu and on T_1^e , it is likely that the relationship between C_{Cu} and T_{1p}^H will not be simple.

The following inversion–recovery data were used to probe the relationship between C_{Cu} and T_{1p}^H ; data are shown grouped according to similar T_1^H 's, and all samples are dried in a vacuum. Figure 17 shows data for CuSPS(7.0) and two blends, 25/75 CuSPS(7.0)/PA and 20/80 CuSPS(11.9)/PA; Figure 18 displays decays associated with CuSPS(2.3), CuSPS(2.3) annealed at 170 °C for 1 h, and 75/25 CuSPS(2.3)/PA. The lines drawn through the data are straight lines with corresponding T_1^H 's given in the figures. Decays vary in exponentiality, some having distinct early-time deviations and some longer-time deviations. The 75/25 CuSPS(2.3)/PA blend, which will be discussed in more detail in the next section, is the most nonexponential, but we expected this on the basis of the spin diffusion behavior of the analogous Zn blend. Table 2 collects the T_1^H data on all the Cu-containing samples looked at. Also listed in Table 2 are the corresponding T_{1p}^H 's, average Cu–Cu distances (assuming a simple cubic lattice and no

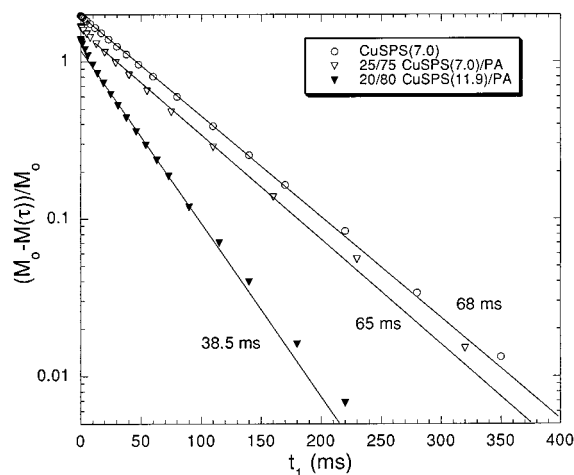


Figure 17. Inversion–recovery data for three indicated materials. The straight lines capture the slopes at about $t_1 = 20$ ms. Qualitatively, the similarity of slopes for both the CuSPS(7.0) ionomer and its 25/75 blend with PA indicates that the unpaired Cu electron relaxes protons in this blend much more efficiently than in the pure ionomer. Ordinate intercepts are all very close to 2.0; however, they have been scaled for clarity.

clustering of Cu ions), and a quantity called RPRE, the relative proton relaxation efficiency assigned to each unpaired Cu electron. RPRE is defined to be proportional to $\rho_H/(C_{Cu}T_{1p}^H)$ where ρ_H is the overall proton density and RPRE = 1 is arbitrarily assigned to the dry CuSPS(11.9) sample. We realize that RPRE can be influenced by many things, among which are changes in T_1^e , in the uniformity of Cu distribution, in the proton density immediately surrounding the Cu, and in the relative importance of direct relaxation versus spin-diffusion-moderated, indirect proton relaxation. Since we do not know how all of these parameters change, RPRE is used only empirically.

On the basis of Figures 13, 17, and 18 and the RPRE values in Table 2, we conclude the following: (a) For the pure ionomers, T_{1p}^H is a very strong function of C_{Cu} . For a 5-fold change in C_{Cu} , there is a 230-fold change in T_{1p}^H . (b) The presence of PA also increases the efficiency per Cu ion for relaxing protons; this is easily

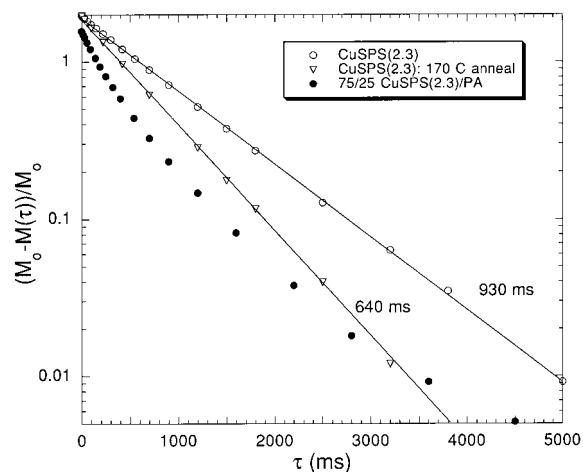


Figure 18. Inversion–recovery data for three indicated materials. Annealing of the CuSPS(2.3) ionomer shortens T_1^H . Straight lines capture the slopes at about 100 ms. The data for the 75/25 CuSPS(2.3)/PA blend are the most nonexponential.

seen in Figure 17 where the CuSPS(7.0) ionomer has the same average T_1^H as a blend sample with a higher proton density and only 25% as much CuSPS(7.0). (c) Annealing at 170 °C for 1 h shortens T_1^H in the CuSPS(2.3) sample. Similar annealing for the CuSPS(11.9) ionomer caused no change (data not shown).

If one postulated the simple relationship, $T_{1p}^H \propto (C_{Cu})^{-\alpha}$, then this limited data on the pure, unannealed ionomers would suggest that $3.2 < \alpha < 3.5$. Theoretical treatments by Blumberg²⁵ describing the relationship between T_{1p}^H and the concentration of electron spins predict that $\alpha = 1$, in both the fast- and the intermediate-spin-diffusion regimes. This theory assumes that the paramagnetic centers are dilute and no clustering occurs. Blumberg also verified his prediction experimentally for NH_4HSO_4 doped with Cr^{3+} . Our CuSPS(11.9) sample has a Cu concentration about 40 times higher than the highest concentration of Cr^{3+} that Blumberg used; therefore, $\alpha = 1$ probably does not apply. While the apparent α for CuSPS decreases a little as the Cu becomes more dilute, the observed range of α in CuSPS is far from unity. Most likely this strong dependence reflects a change in T_1^e as the degree of ion aggregation changes. Even if we do not fully understand the origin of the observed change in T_{1p}^H with C_{Cu} , we can still use these observations in an empirical way to extract a dispersion in local C_{Cu} values (averaged on the 14 nm scale) given the observed dispersion of a factor of 2 in T_1^H ($\approx T_{1p}^H$ for CuSPS(11.9)). Using the conservative choice, $\alpha = 3.0$, the implied dispersion in C_{Cu} , averaged over domains of about 14 nm, is 1.26 for CuSPS(11.9). Thus, any partitioning of the MSPS(11.9) chains, based on different S_i values, over domains significantly larger than 14 nm is only modest.

We speculate that the observed change in T_{1p}^H with annealing for the CuSPS(2.3) sample arises because annealing increases the average number of Cu atoms in the Cu aggregates. On the basis of entropic arguments and the favorable energetics of ion–ion interactions, we would expect the aggregate size in the pure ionomers to increase with increasing Cu concentration. Similarly, in the blends, we would expect the strong Cu–amide interaction to reduce aggregate size because the presence of the PA forces a dilution and a subsequent weakening of the ion–ion interactions that hold

the aggregate together; moreover, from an entropic point of view, the placement of a PA chain in the vicinity of an aggregate of a given size unfavorably reduces the entropy of the included MSPS polymer chains, thereby causing the aggregate to become smaller. (Phase separation of blends of pure PA and PS also indicates no important PS/PA enthalpic attraction.) The reduction of T_1^H with 170 °C annealing observed in the CuSPS(2.3) sample, if explained as an increase in cluster size, suggests that the original sample was not at equilibrium energetically since more extensive aggregation is not an expectation from entropy arguments alone. In contrast, the lack of change of T_1^H for the CuSPS(11.9) sample upon similar annealing suggests either that it is close to equilibrium or that 170 °C is not adequate to provide the molecular mobility needed for further equilibration.

4. Probing the Heterogeneity of Decoration in 75/25 CuSPS(2.3)/PA. Recall that the CSB spin diffusion data for 75/25 ZnSPS(2.3) gave a large asymptote (0.69) in the standardized spin diffusion plot (Figure 8). This asymptote suggested a small amount of PA/ZnSPS mixing in at least one phase; however, from these data alone one cannot tell how many phases are mixed, and if one phase is quite pure, is it the ZnSPS or the PA component which forms this pure phase? From Table 1, we see that the average T_1^H 's of the ZnSPS and PA components were 1410 and 743 ms. Comparing these T_1^H 's with the T_1^H of the pure components in Table 1 strongly suggested that if one phase were pure, it was the ZnSPS. This conclusion was also borne out analyzing line shapes (not shown) as a function of t_1 in an inversion–recovery experiment; i.e., the slower-to-recover spins had a line shape dominated by the ZnSPS line shape. If we then assumed that the asymptote could be interpreted in terms of a mixed phase containing all of the PA and some fraction of the ZnSPS (where some PA was further segregated as crystalline PA within this phase) and a pure phase consisting of the remainder of the ZnSPS, then the average stoichiometry of the mixed phase was computed to be 27/73 ZnSPS/PA where only 12% of the ZnSPS chains would be participating in the mixed phase. This 12% of the ZnSPS was somewhat less than, but of the same order as, the percentage (22%) of chains (see Figure 12) that was computed to have two or more sulfonate sites per chain. Thus, for the reasons mentioned earlier, we thought the probability reasonable that there would be a partitioning of the ZnSPS chains in this blend; i.e., more decorated chains would be found in the mixed phase and less decorated chains would exist in the pure ZnSPS phase. This is what we sought to establish using the analogous 75/25 CuSPS(2.3)/PA blend, expecting that the morphologies of these Zn and Cu analogues would be very similar.

The inversion–recovery data for the 75/25 CuSPS(2.3)/PA sample, both before and after annealing at 130 °C, are shown in Figure 19. Curve fits to the data for $t_1 > 30$ ms are also analyzed for the unannealed sample using a three-exponential fit and for the annealed sample using a two-exponential fit. We focus attention on the unannealed sample since this specimen is expected to mimic the 75/25 ZnSPS(2.3)/PA blend. Elimination of the first 30 ms of data for our analysis allowed for the establishment of a steady-state proton-polarization gradient between the crystalline PA and the surrounding, noncrystalline regions (see Figure 10). Included as insets in Figure 19 are spectra for the unannealed blend (a) and the pure blend components

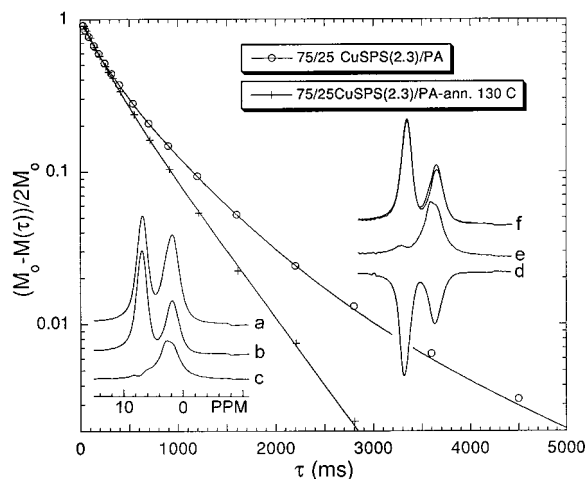


Figure 19. Exponential fits to the inversion–recovery data for both the unannealed and the annealed samples of 75/25 CuSPS(2.3)/PA. A three-exponential fit was required for the unannealed-sample data (amplitudes and corresponding T_1^H 's are 0.397**, 205 ms; 0.547, 586 ms; and 0.045, 1600 ms**, where the quantities with “**” are fixed during the fit.) A two-exponential fit gave good agreement for the annealed-sample data (0.397**, 223 ms; 0.592, 498 ms). Insets show MP spectra of the blend (a), the pure CuSPS(2.3) ionomer (b), and the PA (c). Spectra d and e are respectively inversion–recovery line shapes at $t_1 = 160$ and 340 ms, while spectrum f is a superposition of the CuSPS(2.3) MP spectrum and the difference line shape for the blend generated from the line shapes at 3.6 and 1.0 s. Spectrum f demonstrates that almost all of the PA intensity has relaxed within 1 s in the inversion–recovery spectra. See text for further details.

(b, c). On the right in Figure 19, two inversion–recovery spectra and a difference spectrum are shown. The inversion–recovery spectra are taken at $t_1 = 160$ ms (d) and 340 ms (e) and correspond approximately to the PA and CuSPS nulls. It is clear that the PA relaxes faster, on average, than the CuSPS. The difference spectrum (f) represents the growth of magnetization between 1 and 3.6 s; i.e., this is the later-recovering magnetization. Superposed on this difference spectrum is a scaled version of the CuSPS(2.3) spectrum. As can be easily seen, almost all of the PA intensity has recovered before $t_1 = 1$ s. Since there is little PA contribution to this difference spectrum, it is clear that the longer- T_1^H component is near-pure SPS, as was true in the analogous Zn-containing blend.

The fits in Figure 19 are quite good; however, these are not the most general fits. Rather, these fits assume that the shorter T_1^H is assignable to a semicrystalline, mixed phase with a 27/73 overall composition. That assumption fixes the amplitude of this shorter- T_1^H component at 0.397. Multiexponential analysis then dictates that the T_1^H of this component is about 200 ms for both the annealed and unannealed samples. The principal longer- T_1^H component in the unannealed sample has a T_1^H of about 600 ms; the T_1^H of the longest- T_1^H component was set to 1530 ms, since this was the T_1^H associated with pure, undecorated PS chains, should the latter be present. The fit yielded only a very small (0.045) amplitude associated with this long decay, indicating that, at best, a very minor portion of the undecorated PS chains phase separate into large domains.

If we assume, as in the analogous Zn-containing blend, that the phases are large and negligible spin diffusion between phases takes place, then the 200 ms T_1^H is an accurate reflection of the T_1^H of this phase.

Using the corresponding T_1^H of 270 ms from Table 2, we can further calculate an RPRE value, assuming for the moment that no S_I -based partitioning occurs and that the mixed phase possesses a fixed, 27/73 stoichiometry. The fact that some PA crystallinity exists is expected to be a minor perturbation on the RPRE calculation supposing that the time scale (see Figure 10) for spin diffusion between CR and NC phases is probably less than 20% of this shorter T_1^H . The “no-partitioning” RPRE value is 1.14, which is in the range of the RPRE values observed in the PA-rich blends in Table 2. If there were the maximum C_{Cu} enhancement, i.e., 2.93 times the average C_{Cu} , for this assumed 27/73 phase composition, then RPRE would be only 0.39, i.e., anomalously low. On the other hand, the 600 ms T_1^H associated with the major portion of the assumed “pure-SPS” phase is shorter than the 930 ms T_1^H seen in pure CuSPS(2.3). A trace of PA in this phase could easily shorten the T_1^H of this phase based on the contrast in RPRE values in Table 2 for ZnSPS(2.3) versus the blends.

Under the assumption that the phase composition for the 75/25 CuSPS(2.3)/PA is exactly the same as the for the analogous Zn-containing blend, the deduction from the principal T_1^H components is that there is very little partitioning of the more decorated SPS chains into the mixed phase. Since this result goes against our intuition, we comment briefly on the critical assumptions leading to this conclusion and why, in the end, we believe this has not been an unambiguous test of partitioning.

The key issue is, again, that when a curve has multiple exponential components, one cannot deduce both the amplitudes and time constants with high accuracy when the time constants differ by no more than a factor of about 3. Hence, we cannot know the component amplitudes with sufficient accuracy to define the true mixed-phase stoichiometry in this Cu-containing blend. Thus, fits to the inversion–recovery data, based on, say, a 10/90, instead of a 27/73, CuSPS/PA stoichiometry, are indistinguishable from the fits shown in Figure 19 since the proton fraction associated with this mixed phase only changes from 0.397 to 0.338. A T_1^H of 200 ms associated with such a 10/90 stoichiometry would imply a very significant enhancement (≈ 2.9 , maximum possible is 3.8) of decoration density in the mixed phase over the average value. Again, with respect to the T_1^H of the longer-relaxing component(s) the analysis of the inversion–recovery is not good enough to eliminate the possibility that a trace of PA is included in this phase. Hence, the longer T_1^H cannot be interpreted firmly in terms of C_{Cu} .

For this unannealed 25/75 CuSPS(2.3)/PA blend we conclude the following: (a) the PA-rich, semicrystalline phase definitely contains some CuSPS because its T_1^H is much shorter than for pure PA; (b) there is an S_I -based partitioning of the SPS chains into the mixed phase only if the mass fraction of SPS in the mixed phase is substantially less than the 27% found in the analogous Zn-containing blend; and (c) if the small-amplitude, longest- T_1^H component corresponds to undecorated PS chains which phase separate into large domains of pure PS, then 16% is the maximum fraction of these undecorated PS chains which exist in such regions. However, this correspondence is suspect because annealing at 130 °C appears to eliminate such regions rather than foster their growth.

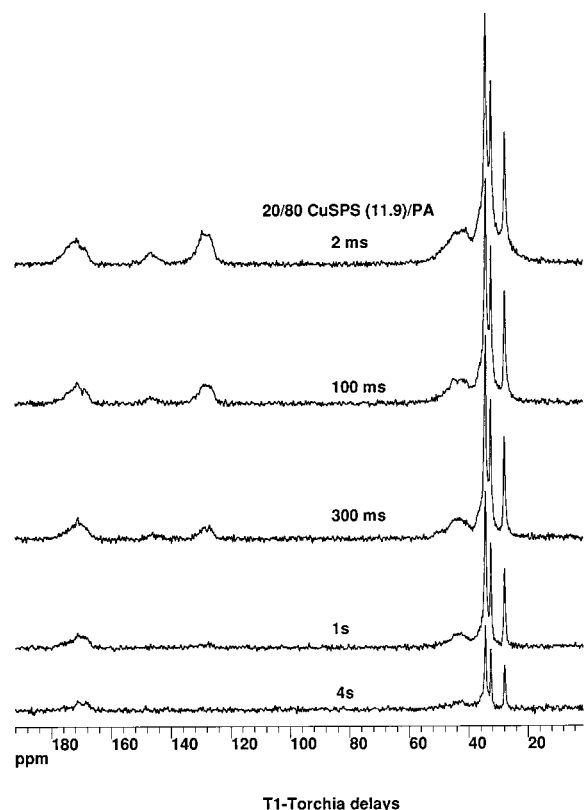


Figure 20. The 25 MHz ^{13}C CPMAS spectra associated with various delays in a T_1^{C} experiment using the method of Torchia (ref 44). In this 20/80 CuSPS(11.9)/PA blend, T_1^{C} for the five protonated carbons (≈ 126 ppm) and the unprotonated aromatic carbon (≈ 146 ppm) of the CuSPS is similar, indicating the dominance of the electron–nuclear mechanism for T_1^{C} . Note the persistence of the crystalline-PA lines, indicating that the crystalline PA is much more distant from the Cu sites, as expected.

5. Miscellaneous Deductions. Given that the inversion–recovery data for the CuSPS(11.9) ionomer could be analyzed in terms of an implied distribution of C_{Cu} , do the data for the CuSPS(7.0) and CuSPS(2.3) ionomers hold the same promise? The information content for these latter samples is meager. Beyond the initial nonexponentiality, decays are quite exponential. Considering the statistics of decoration summarized in Table 2, where the fraction of undecorated chains varies from 6% to 41%, the data indicate that large domains of undecorated chains are absent (“large” meaning of a dimension such that spin diffusion with Cu-containing domains on a time scale of T_1^{H} would be minimal). Also, considering this exponentiality, if any significant segregation of domains based on level of decoration occurs, this segregation occurs on a small enough scale such that deviations from sample-average stoichiometries, averaged over dimensions of about 26 nm in CuSPS-(7.0) and 100 nm in CuSPS(2.3), are probably no greater than 20%.

We did some measurements of ^{13}C longitudinal relaxation, T_1^{C} , using the sequence of Torchia,⁴⁴ in undried and dried CuSPS(11.9), in dried 20/80 CuSPS(11.9)/PA, and, for a diamagnetic reference, in dried ZnSPS(11.9). Blend spectra, as a function of the time ($=t_1$) between magnetization preparation and observation, are shown in Figure 20, and selected data are plotted against $t_1^{1/2}$ in Figure 21. In the absence of ^{13}C – ^{13}C spin diffusion, such plots are expected²⁵ to be linear at earlier times when paramagnetic centers are present. ^{13}C – ^{13}C spin

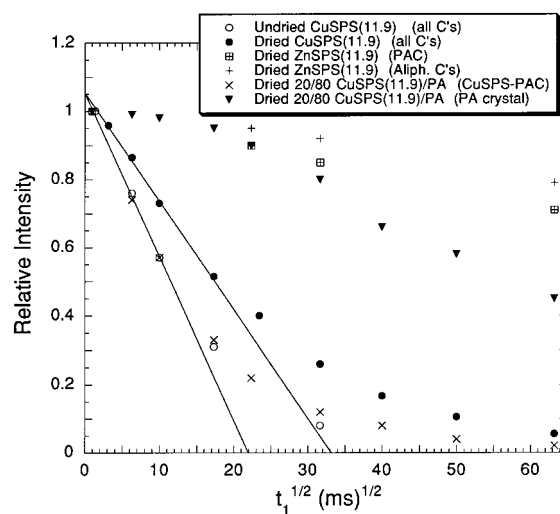


Figure 21. Plots of intensity versus $t_1^{0.5}$ in a Torchia-type T_1^{C} experiment performed on dried and undried CuSPS(11.9), on the reference, dried ZnSPS(11.9), and on the blend, 20/80 CuSPS(11.9)/PA. Linear early-time behavior is expected for randomly spaced paramagnetic relaxation sources which directly relax ^{13}C nuclei in the absence of ^{13}C – ^{13}C spin diffusion; straight lines approximate these slopes. “PAC” stands for protonated aromatic carbons of the SPS, and “Aliph” refers to the aliphatic carbons. Among other things, these data show that T_1^{e} changes in the presence of water and, most likely, via blending with PA.

diffusion should be a minor perturbation over the first second of decay.⁴⁵ Decays for the SPS carbons in the three paramagnetic samples are quite linear at earlier times.

Just a few deductions will be made from these data. First, all PS carbons relax at the same rate in the presence of the Cu and at a rate much faster than for the same carbons in diamagnetic ZnSPS(11.9). Therefore, at early times, direct electron–carbon interactions dominate the relaxation. Second, a majority of the spins are close enough to the paramagnetic centers to be relaxed within 1 s. An average distance between paramagnetic centers of 3.2 nm is reasonable in this context. Third, the explanation for the observed change in T_1^{H} in CuSPS(11.9) upon drying is now apparent; i.e., the presence of water changes T_1^{e} such that relaxation efficiency is enhanced. (If T_1^{e} remained the same and the water protons were additionally polarized, thereby shortening T_1^{H} , then this additional water-proton polarization would have less influence on T_1^{C} than it would have on T_1^{H} . In contradiction to this expectation, T_1^{H} and T_1^{C} increase by about the same proportion upon drying.) Fourth, T_1^{C} relaxation of the PS carbons in dried CuSPS(11.9) is longer than for the dried 20/80 CuSPS(11.9)/PA blend. This trend is consistent with RPRE values; however, changes in T_1^{C} cannot be interpreted directly in terms of T_1^{e} since changes in cluster size (and in the distribution of PS about each Cu site) is simultaneously occurring. Nevertheless, the qualitative deduction is that the T_1^{e} s in dry CuSPS-(11.9) and the dry blend are not very different. Fifth, using eqs 5 and 15 of Blumberg²⁵ to interpret the observed ^{13}C relaxation time of CuSPS(11.9) along with the assumption that this ionomer consists of aggregates of 10 ions spaced at 3.2 nm allows a rough estimate of T_1^{e} in the range from 4×10^{-8} to 10^{-9} s for dry CuSPS-(11.9). This is within the general range that had been anticipated for Cu electrons. As a check on this estimate of T_1^{e} , we also used this T_1^{e} range to predict the expected

T_1^H range using eq 9 of Blumberg; these predicted values fell within the factor of 1.5 of the observed T_1^H . When T_1^e is in this range, most spectral broadening for surrounding protons can be described by replacing the magnetic moment of the electron with its smaller, T_1^e -averaged moment, consistent with the observation that more than 95% of the protons are visible in a multiple-pulse spectrum. Also, for dry CuSPS(11.9) the nonspinning T_{1xz} decay, which is sensitive to local magnetic fluctuations in the mid-kilohertz frequency range,²⁴ was measured. Although this decay was not strictly exponential, decay by the factor e^{-1} occurred in 10 ms, i.e., in a time very comparable to T_1^H (such decay took 20 ms in ZnSPS(11.9)). Even though T_1^H is strongly influenced by spin diffusion and, to a first approximation, T_{1xz} decay occurs in the absence of spin diffusion, the comparability of T_1^H and T_{1xz} suggests that T_1^e cannot be much longer than the T_1^e ($=8 \times 10^{-10}$ s) associated with the T_1^H minimum. Therefore, 10^{-9} s is probably closer to T_1^e than is 4×10^{-8} s.

In Figure 7 there seemed to be a trend in the ZnSPS-(11.9)/PA blends that as the PA mass fraction increased, the long-time spin diffusion data deviated more from full spin equilibrium, implying some large-scale compositional inhomogeneity. The 20/80 CuSPS(11.9)/PA sample offers the chance to determine whether this inhomogeneity could possibly arise from some PA which segregated into a large, pure phase. If that were true, there should be some minor fraction of the protons that exhibited a T_1^H in the 600–1000 ms range, typical of pure PA. In the inversion–recovery data of Figure 17 there is no such component whose relative intensity constitutes more than 0.5% of the total intensity; hence, there is no evidence for pure PA regions exceeding 30 nm in dimension.

Table 2 includes several of the deductions which pertain to the Cu-containing ionomers and blends.

Summary and Conclusions

Chemical-shift-based (CSB) proton spin diffusion data were acquired for blends of a low-MW (≈ 4000) metal-sulfonated poly(styrene) (MSPS) and a methylated poly-(amide) (PA) of $M_n = 25$ kg/mol and $M_w = 65$ kg/mol. The metals were Zn and Cu; the sulfonate mole fractions in the MSPS materials investigated were 11.9, 7.0, and 2.3%. Without sulfonate decoration, these polymers are incompatible and phase separate. The goal of this study was to learn more about morphology in these MSPS-(*n*)/PA blends.

Zn and Cu are similar in ion size and interaction strength; therefore, blends of Zn or Cu with comparable stoichiometries ought to show similar morphologies. Yet, from an NMR point of view, protons in these blends behave very differently. The Zn blends are diamagnetic; the Cu blends are paramagnetic. Thus, the influence of the unpaired electron of Cu on the proton relaxation was used to test for the uniformity of ion concentration in ionomers and to test for large domains of PA or undecorated PS chains in the blends.

For blends at the highest decoration level (11.9%), the ZnSPS seemed to mix very intimately with PA in those regions where mixing occurred as evidenced by the rapid spin diffusion between the ZnSPS and PA protons. For ZnSPS mass fractions of 0.5 and 0.75, PA crystallinity is suppressed, and there is no evidence of more than one phase. Below a ZnSPS mass fraction of 0.5 and beginning with a mass fraction of 0.35, PA crystallinity

appears; PA crystallites obviously represent domains of pure-PA composition. The fraction of PA crystallinity increases as the mass fraction of PA increases. Moreover, as the PA fraction increases, there is some indication in the CSB spin diffusion data of larger-scale compositional inhomogeneity; nevertheless, there is no evidence in analogous Cu-containing blends of a pure-PA phase developing outside the boundaries of each PA crystallite. Thus, the nucleation and growth of PA crystallites seems to occur in the vicinity of, or directly out of, a mixed ZnSPS(11.9)/PA phase, the crystallites achieving larger dimensions when the concentration of the metal sulfonate groups diminishes.

The existence of and the fraction of PA crystallinity are more evident from the ¹³C CPMAS spectra than from the CSB spin diffusion plots. In addition, T_{1xz} -based spin diffusion data offered further insight into the morphologies of the 25/75 ZnSPS(7.0)/PA and the 25/75 and 18/82 ZnSPS(11.9)/PA semicrystalline blends in that a considerable amount of spin equilibration between crystalline PA and ZnSPS protons occurs over the 30–40 ms range, implying average overall repeat distances in the range 20–25 nm. In addition, the existence of an interface region of depleted ZnSPS concentration is demonstrated. Thus, the noncrystalline region surrounding the PA crystallites is by no means uniform in ZnSPS concentration.

Some aging studies were carried out on the 18/82 ZnSPS(11.9)/PA blend. Aging occurs with time, but the presence of water strongly promotes aging, possibly by imparting more mobility to the PA chains and possibly also by lowering the activation barrier for dissociation of the Zn–amide bond. Interestingly, the 20–25 nm characteristic distance, which typifies the ZnSPS(11.9)/PA blends at the higher PA mass fractions, does not change perceptibly during aging; aging-related demixing is occurring on a smaller scale. Demixing is seen as a growth of each PA crystallite, including its boundary of depleted ZnSPS. Thus, the ZnSPS is forced into smaller, more concentrated zones. The stability of the overall repeat distance (a kind of structure pinning) is probably, in part, related to the tenacity of the ion–amide interaction and in part to the anchoring action of those PA chains that participate in the crystallites.

The “structure pinning” just mentioned is qualitatively different from that recently observed⁴⁶ by light scattering in lightly decorated 50/50 LiSPS(*n*)/PA blends ($n = 4.0$ – 9.5) above the lower critical solution temperature (LCST). There, phase separation into PA-rich and LiSPS-rich domains occurred, but the growth of domains was arrested after a modest time and the average domain size was a function of annealing temperature. To explain the structure pinning, the authors of that work invoked a gelation phenomenon associated with either the building up of ionomer aggregates or a concentrating of ion–amide interactions in the ionomer-rich phase. We do not venture to comment, on the basis of our observations, on this gelation mechanism. However, we can comment on whether our samples were, at any time, subjected to temperatures above their LCST's so that some of the heterogeneities of composition may have had their origin in such phase separation. Our best assessment, based on the reported⁴⁶ LCST's, is that only the 75/25 CuSPS(2.3)/PA sample, which was heated to 130 °C, might have been subjected to such phase separation. The data of Figure 19, while not definitive on this point, show a trend in T_1^H opposite to

that expected if annealing at 130 °C caused further phase separation. Also, we used a lower molecular mass for the MSPS, compared to their LiSPS, and we used the more strongly interacting Zn^{2+} and Cu^{2+} cations,³⁶ compared to their Li^+ cation; both considerations, at constant composition and decoration level, should increase our LCST's compared to theirs and reduce the chances that any of our samples were raised above their respective LCST's.

As one lowers the mole fraction of decorations to 7.0% and 2.3%, more heterogeneity of composition is revealed in the CSB spin diffusion experiments on these blends. While the 75/25 ZnSPS(7.0)/PA blend is mixed quite intimately and has no PA crystallinity, the corresponding 25/75 blend shows compositional inhomogeneity over multiple distance scales. The 75/25 ZnSPS(2.3)/PA blend shows PA crystallinity and a large-scale compositional inhomogeneity. The latter is determined to consist of a mixed, semicrystalline phase containing most of the PA plus only about 10–15% of the ZnSPS and a second phase which contains the balance of the ZnSPS and, possibly, a very small amount of PA. We tried to test, using an analogous 75/25 CuSPS(2.3)/PA blend, whether the average decoration level of those MSPS chains in the mixed phase was significantly higher than the average MSPS decoration level. Assuming identical morphologies and phase stoichiometries for the Zn and Cu blends, it was concluded, on the basis of mainly the T_1^H of the faster-relaxing component, that there was little, if any, decoration-dependent partitioning of SPS chains in the mixed phase. However, it was also shown that the existence or nonexistence of such partitioning depended critically on the assumed stoichiometry of the mixed phase and that the data were inadequate for verifying that stoichiometry. Hence, the foregoing conclusion is not proven beyond doubt. A future unambiguous determination of whether the more decorated ionomer molecules are preferentially incorporated into the mixed phase will provide a key insight into the thermodynamics of phase separation as well as domain growth in these blends.

For the pure CuSPS(11.9) ionomer, spin diffusion behavior at short times could be used to argue that the 3.2 nm periodicity seen in the small-angle X-ray scattering data is associated with the average distance between paramagnetic centers. Furthermore, from simple geometric arguments, these centers then correspond to aggregates each containing about 10 metal ions. In addition, for this pure ionomer, we attempted to estimate the dispersion in Cu concentration from the distribution of T_1^H 's deduced from the inversion-recovery data. Taking account of spin diffusion in an ad hoc manner and connecting T_1^H data with Cu concentration using T_1^H data for all of the ionomers, it was concluded that if one averaged Cu concentration over distance scales of 14 nm, the dispersion in averaged Cu concentration would be within a factor of 1.3 for 95% of the domains. The existence of a dispersion of Cu concentration on this distance scale is consistent with SAXS observations where small-angle scattering, related to the presence of the metal ion and having no observable maximum, is seen.^{40–42} These SAXS observations led to the postulate⁴² that the heterogeneity of ion distribution extends from nanometers to microns. We do not disagree with these authors for in this study we have tried to define the magnitude of this heterogeneity in Cu concentration averaged over a particular

distance scale. The lack of a SAXS maximum implies that inhomogeneity is not confined to the 14 nm scale; smaller dispersions in average concentration are expected on scales bigger than 14 nm and larger dispersions over smaller distances.

Finally, in view of the strong reported⁴⁷ tendency for lightly sulfonated HSPS(1.7) to phase separate from undecorated, perdeuterated PS (M_w 's $\approx 2 \times 10^5$), even at stoichiometries as disparate as 95/5, we were surprised that we saw no evidence for undecorated PS chains separating from their decorated counterparts, especially in the CuSPS(2.3) ionomer or the 75/25 CuSPS(2.3)/PA blend where about 40% of the SPS chains are undecorated. Whether this difference has to do with our much lower M_w , or metal ion versus free acid form, or with domain size and preparation history is a matter of speculation, and more work must be done to sort this out.

In this paper we have shown that NMR can give unique insights into the morphology and phase separation of blends of ionomers and semicrystalline polymers. These insights include information about phase stoichiometry in phase-separated blends (including the nonexistence of large domains of pure PA), the intimate level of mixing in the mixed phases, and a description of crystal growth and aging in terms of structure pinning at one length scale and demixing on a smaller length scale. In addition we were able to estimate compositional inhomogeneity in a pure ionomer. In combination with other characterization techniques (e.g., X-ray), NMR also offers the opportunity to use blends, involving paramagnetic ionomers, to pursue the hypothesis that the mixed phase attracts chains with higher-than-average levels of decoration. Paramagnetic doping of blends is a useful approach, but interpretations must be carefully made.

Acknowledgment. The authors thank Dr. J. D. Barnes for his help in obtaining SAXS scattering data. We also acknowledge the Polymer Program of the National Science Foundation for partial support of this work (Grant DMR 97-12194).

References and Notes

- (1) Odian, G. *Principles of Polymerization*, 2nd ed.; Wiley: New York, 1981; Chapter 1.
- (2) Kuphal, J. A.; Sperling, L. H.; Bobeson, L. M. *J. Appl. Polym. Sci.* **1991**, *42*, 1525.
- (3) Coleman, M. M.; Hu, J.; Painter, P. C. *ACS PMSE Prepr.* **1988**, *59*, 321.
- (4) Ellis, T. S. *Polym. Eng. Sci.* **1990**, *30*, 998.
- (5) Eisenberg, A., Ed.; *Ions in Polymers; Adv. Chem. Ser.* **1980**, No. 187.
- (6) Eisenberg, A.; Yeo, S. C. *J. Appl. Polym. Sci.* **1977**, *21*, 875.
- (7) Weiss, R. A.; Lundberg, R. D.; Werner, A. *J. Polym. Sci., Polym. Chem.* **1980**, *18*, 3427.
- (8) Weiss, R. A.; Lu, X. *Polymer* **1994**, *35*, 1963.
- (9) Lu, X.; Weiss, R. A. *Mater. Res. Soc. Proc.* **1991**, *215*, 29.
- (10) Molnar, A.; Eisenberg, A. *Polymer* **1991**, *32*, 370.
- (11) Molnar, A.; Eisenberg, A. *Macromolecules* **1992**, *25*, 5774.
- (12) Smith, P.; Eisenberg, A. *J. Polym. Sci., Polym. Phys. Ed.* **1988**, *26*, 569.
- (13) Gao, Zhisheng; Molnar, A.; Morin, F. G.; Eisenberg, A. *Macromolecules* **1992**, *25*, 6460.
- (14) Lu, X.; Weiss, R. A. *Macromolecules* **1993**, *26*, 6583.
- (15) Zhang, X.; Natansohn, A.; Eisenberg, A. *Macromolecules* **1990**, *23*, 412.
- (16) Waugh, J. S.; Huber, L. M.; Haeberlen, U. *Phys. Rev. Lett.* **1968**, *20*, 180.
- (17) Rhim, W.-K.; Elleman, D. D.; Vaughan, R. W. *J. Chem. Phys.* **1973**, *59*, 3740.

- (18) Mansfield, P.; Orchard, J.; Stalker, D. C.; Richards, K. H. B. *Phys. Rev.* **1973**, *B7*, 90.
- (19) Caravatti, P.; Neuenschwander, P.; Ernst, R. R. *Macromolecules* **1985**, *18*, 119.
- (20) Caravatti, P.; Neuenschwander, P.; Ernst, R. R. *Macromolecules* **1986**, *19*, 1895.
- (21) Campbell, G. C.; VanderHart, D. L. *J. Magn. Reson.* **1992**, *96*, 69.
- (22) VanderHart, D. L.; McFadden, G. B. *Solid State Nucl. Magn. Reson.* **1996**, *7*, 45.
- (23) Havens, J.; VanderHart, D. L. *Macromolecules* **1985**, *18*, 1663.
- (24) Vega, A. J.; Vaughan, R. W. *J. Chem. Phys.* **1978**, *68*, 1958.
- (25) Blumberg, W. E. *Phys. Rev.* **1960**, *119*, 79.
- (26) Huang, S. J.; Kozakiewicz, J. *J. Macromol. Sci., Chem.* **1981**, *A15*, 821.
- (27) Certain commercial companies are named in order to specify adequately the experimental procedure. This in no way implies endorsement or recommendation by NIST.
- (28) Makowski, H. S.; Lundberg, R. D.; Singhal, G. H. US Patent 3,870,841, 1975.
- (29) VanderHart, D. L.; Pérez, E. *Macromolecules* **1986**, *19*, 1902.
- (30) Hexem, J. G.; Frey, M. H.; Opella, S. J. *J. Chem. Phys.* **1982**, *77*, 3847.
- (31) Zumbulyadis, N.; Henrichs, P. M.; Young, R. H. *J. Chem. Phys.* **1981**, *75*, 1603.
- (32) Kwei, T. K.; Dai, Y. K.; Lu, X.; Weiss, R. A. *Macromolecules* **1993**, *26*, 6583.
- (33) VanderHart, D. L. *Macromolecules* **1994**, *27*, 2837.
- (34) Vega, A. J.; English, A. D.; Mahler, W. *J. Magn. Reson.* **1980**, *37*, 107.
- (35) Galambos, A. F.; Stockton, W. B.; Koberstein, J. T.; Sen, A.; Weiss, R. A. *Macromolecules* **1987**, *20*, 3091.
- (36) Feng, Y.; Schmidt, A.; Weiss, R. A. *Macromolecules* **1996**, *29*, 3909.
- (37) Feng, Y. Ph.D. Thesis, University of Connecticut, 1995.
- (38) Swift, T. J. In *NMR of Paramagnetic Molecules*; La Mar, G. N., Horrocks, Jr., W. DeW., Holm, R. H.; Eds.; Academic Press: New York, 1973; Chapter 2.
- (39) De Gennes, P.-G. *J. Phys. Chem. Solids* **1958**, *7*, 345.
- (40) Ding, Y. S.; Hubbard, S. R.; Hodgson, K. O.; Register, R. A.; Cooper, S. L. *Macromolecules* **1988**, *21*, 1698.
- (41) Grady, B. P.; Matsuoka, H.; Nakatani, Y.; Cooper, S. L.; Ise, N. *Macromolecules* **1993**, *26*, 4064.
- (42) Li, Y.; Peiffer, D. G.; Chu, B. *Macromolecules* **1993**, *26*, 4006.
- (43) Schmidt-Rohr, K.; Spiess, H. W. *Multidimensional Solid-State NMR and Polymers*; Academic Press: London, 1994; Chapter 13.
- (44) Torchia, D. A. *J. Magn. Reson.* **1978**, *30*, 613.
- (45) VanderHart, D. L. *J. Magn. Reson.* **1987**, *72*, 13.
- (46) Feng, Y.; Weiss, R. A.; Han, C. C. *Macromolecules* **1996**, *29*, 3925.
- (47) Beck Tan, N. C.; Liu, X.; Briber, R. M.; Peiffer, D. G. *Polymer* **1995**, *36*, 1969.

MA991545K